INVESTIGATION OF VENTRICULAR ASSIST DEVICE INFLOW CANNULA CONFIGURATIONS WITHIN SINGLE VENTRICLE HEARTS

A Dissertation

by

ANNE-MARIE GINN-HEDMAN

Submitted to the Graduate and Professional School of
Texas A&M University
in partial fulfillment of the requirements for the degree of

DOCTOR OF PHILOSOPHY

Chair of Committee,	Fred Clubb, Jr.
Committee Members,	Saurabh Biswas
	John Criscione
	Bradley Weeks
Head of Department,	Michael McShane

May 2022

Major Subject: Biomedical Engineering

ABSTRACT

Ventricular assist devices (VADs) are life-saving devices that provide cardiac support to failing hearts. However, over half of VADs are malpositioned which can lead to serious complications such as thrombus formation, pump failure, and even patient death. Therefore, this work investigates the relationship between VAD inflow cannula position and potential for thrombus formation, and proposes a surgical method for minimizing instances of VAD mispositioning within single ventricle hearts.

VADS are commonly implanted in either the diaphragmatic or apical configuration. Both configurations were explored; specifically, the effect of the inflow cannula position on fluid flow within the ventricle chamber was assessed via computational fluid dynamics and validated with particle image velocimetry using a mock circulation loop. A new surgical technique involving low-cost image guided surgery was also investigated and evaluated using computational fluid dynamics to predict thrombogenic potential due to implant positioning.

Computational results revealed a greater volume of fluid with thrombogenic potential for the apical inflow cannula configuration. While particle image velocimetry validated overall trends observed in the computational model, specific numerical values differed, suggesting the need for future refinement of both models. Computational analysis also revealed reduced thrombogenic potential for inflow cannulas implanted using image guided surgery rather than traditional surgical techniques. Accordingly, image guided surgery should be considered as a useful tool for optimizing VAD inflow cannula positioning in complex surgical scenarios such as patients with single systemic ventricles.

DEDICATION

Thank you Mom, Dad, and Paul. Love you most.

ACKNOWLEDGEMENTS

I would like to thank my committee chair, Dr. Clubb, and my committee members, Dr. Biswas, Dr. Criscione, and Dr. Weeks for their support throughout this process. I would also like to thank Dr. Staci Jessen Horn for her mentorship.

Thanks also to my colleagues and the faculty/staff within the Biomedical Engineering department, and to my friends at the Cardiovascular Pathology Lab.

Thank you to my friends Lonnie Allen, Brittany Rogers, and M. Sidney Atkins for always encouraging me to take breaks and have fun. Thank you to my sister, Tommy, and Blake for always brightening my day.

Finally, I would like to thank Mom, Dad, and Paul. Thank you, Mom, for always taking care of me. Thank you, Dad, for always inspiring me. And thank you Paul for being my best friend. I could not have done this without you. I love you most, and cannot thank you enough.

CONTRIBUTORS AND FUNDING SOURCES

Contributors

This work was supervised by a dissertation committee consisting of Dr. Fred Clubb, Jr. of the Department of Biomedical Engineering and of the Department of Veterinary Pathobiology, Dr. Saurabh Biswas and Dr. John Criscione of the Department of Biomedical Engineering, and Dr. Bradley Weeks of the Department of Veterinary Pathobiology. The work was also critically reviewed by Dr. Staci Jessen Horn.

The mock circulatory loop was constructed in part by Dr. Thomas Ginn and Paul Hedman, and cannula implantation for the image guided surgery study was supervised by Dr. Kirsten Landsgaard. The patient MRI HLHS data was supplied by members of the Cardiac Atlas Project, specifically Dr. Jeffrey Omens and Dr. Nickolas Forsch. All other work conducted for the dissertation was completed by the student independently.

Funding Sources

This work was supported by the National Science Foundation Graduate Research Fellowship Program Grant Number DGE:1746932 (Ginn-Hedman). This work was also supported in part by the National Heart, Lung, and Blood Institute, National Institutes of Health under Grant #HL121754 (McCulloch/Omens).

NOMENCLATURE

VAD	Ventricular Assist Device
HLHS	Hypoplastic Left Heart Syndrome
CFD	Computational Fluid Dynamics
PIV	Particle Image Velocimetry
IGS	Image Guided Surgery

TABLE OF CONTENTS

Page

LIST OF FIGURES

Page

LIST OF TABLES

Page

1. INTRODUCTION

1.1 Hypoplastic Left Heart Syndrome

Hypoplastic left heart syndrome (HLHS) is a rare but fatal congenital anomaly where the left ventricle of the heart is severely underdeveloped, resulting in a single systemic ventricle (Figure 1-1A) [1]. HLHS has an incidence rate of one in every 5,000 births and if left untreated, has a mortality rate of 95% [2]. In fact, this condition is responsible for approximately 25-40% of all newborn cardiac deaths [1]. Heart transplantation is rarely an option due to the shortage of donors, difficulty in size matching, and long waiting periods. Patients often wait over one hundred days for a donor heart, and even once a match is found, rejection is common – especially in the pediatric population [3]. In order to sustain life, infants must undergo intense surgical revision, or "staged palliation," including the Norwood, Glenn, and Fontan reconstructive procedures [4]. After surgery, the reconstructed single right ventricle (Figure 1-1B) becomes solely responsible for pumping blood through the systemic circulation, which results in increased stress and eventual systolic ventricular dysfunction [5-7]. This dysfunction manifests as low cardiac output, low ejection fraction, high end diastolic volumes and pressures, and decreased contractility [5-7]. Clinically, patients exhibit an exercise intolerance and a protein losing enteropathy [8,9]. Dr. Fontan himself stated that this reconstructive surgery only provides "palliative but not curative" care and that the failing Fontan should be supplemented with additional support [8,9]. Ventricular assist devices (VADs) can provide the circulatory support needed after surgical correction, lowering end diastolic pressures and increasing cardiac output [5-7].

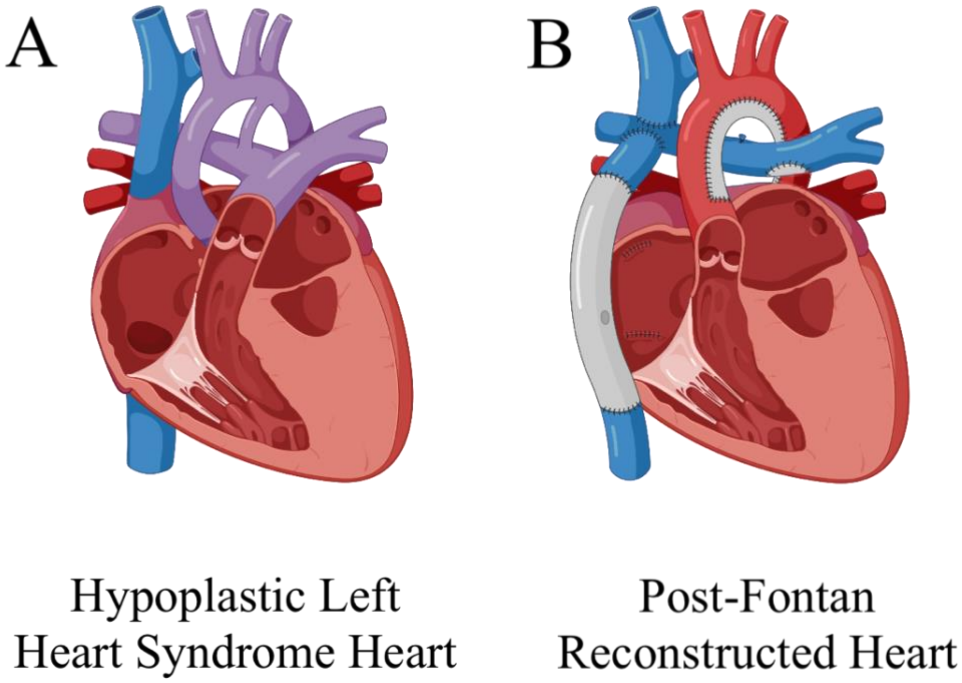

Figure 1-1: Reconstructed HLHS Heart – A heart with hypoplastic left heart syndrome has a severely underdeveloped left ventricle and is incompatible with life (A). Patients with this condition must undergo staged surgical reconstruction in order to live. The final stage of surgical palliation is the Fontan procedure which results in a heart with a single systemic ventricle solely responsible for cardiac support (B). Figure created with BioRender.com.

1.2 Ventricular Assist Devices in Single Ventricle Hearts

Ventricular assist devices (VADs) are life-saving devices that provide cardiac support to failing hearts. Blood enters through the VAD inflow cannula, travels through the pump, and exits through the outflow graft, bypassing the native cardiac circulation [10]. A VAD is usually implanted within a ventricle with its outflow graft connected to the aorta (Figure 1-2); other configurations such as atrial-to-pulmonary artery connections exist, though [10,11]. Two main types of VADs are common – continuous flow and pulsatile flow pumps – and examples include the HeartWare HVAD and Berlin Heart EXCOR, respectively [12]. Both types of VADs have been successfully used for single ventricle support. For example, Meira et al. successfully supported a twelve-year-old HLHS patient on a HeartWare HVAD until transplantation, while Cardarelli et al. supported a two-year-old on a Berlin Heart EXCOR for 183 days until recovery [13,14]. Of note, the average duration of VAD support for single ventricle hearts is approximately 52 days with the Berlin Heart EXCOR as the most commonly implanted VAD [15].

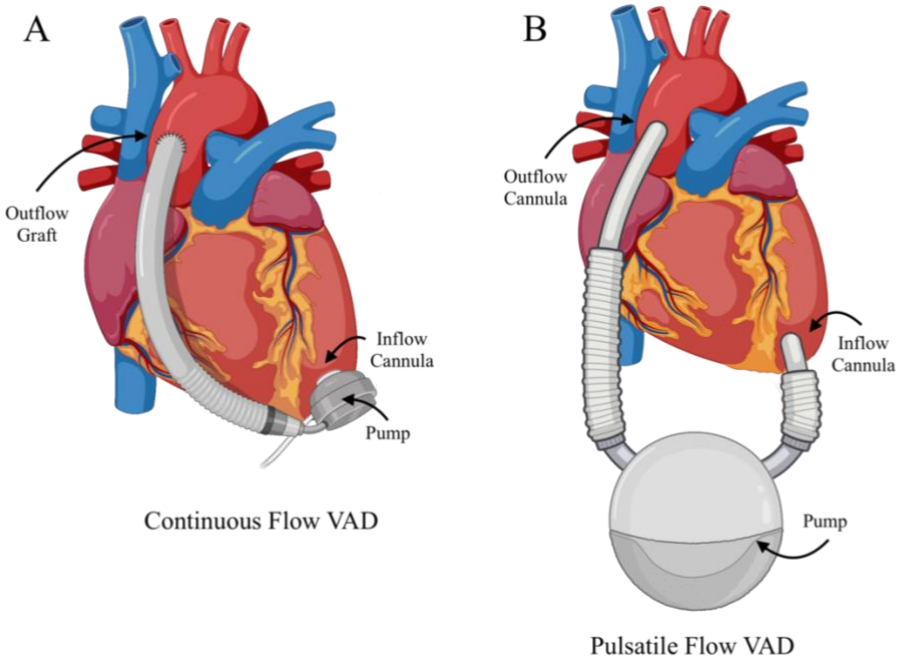

Figure 1-2: Continuous vs. Pulsatile Flow VADS – Ventricular assist devices (VADs) provide cardiac support to failing hearts. Blood flows through the inflow cannula, the pump, and then the outflow graft. There are several types of VADs including continuous flow (A) and pulsatile flow (B) pumps. Figure created with BioRender.com.

1.3 Ventricular Assist Device Inflow Cannula Configurations

Ventricular assist devices are traditionally difficult to implant in patients with HLHS due to their small chest size, unique geometry, and excessive trabeculae [6,16]. Dense trabeculations are common in patients with HLHS and excessive muscular resection is required for VAD implantation [17]. Furthermore, as the heart becomes overloaded and dilates, the apex becomes more difficult to locate [17]. There are two common locations where VAD implantation occurs – the apex of the heart and the diaphragmatic surface of the heart (Figure 1-3). Gregoric et al. popularized implanting the inflow cannula in the diaphragmatic configuration at approximately one-third from the apex to the base of the heart; this is known as "Frazier's Point" (Figure 1-4A) [18]. The philosophy behind this implant technique is that it leads to an unobstructed inflow cannula and results in a more centrally placed VAD. Adamson et al., on the other hand, recommend the more common apical implant configuration where the inflow cannula is pointed toward the outflow valve and parallel to the septum, for the case of a left ventricular implant (Figure 1-4B) [19]. There is a significant debate over which VAD placement leads to better clinical outcomes, and which configuration is better suited for pediatric patients [18,19].

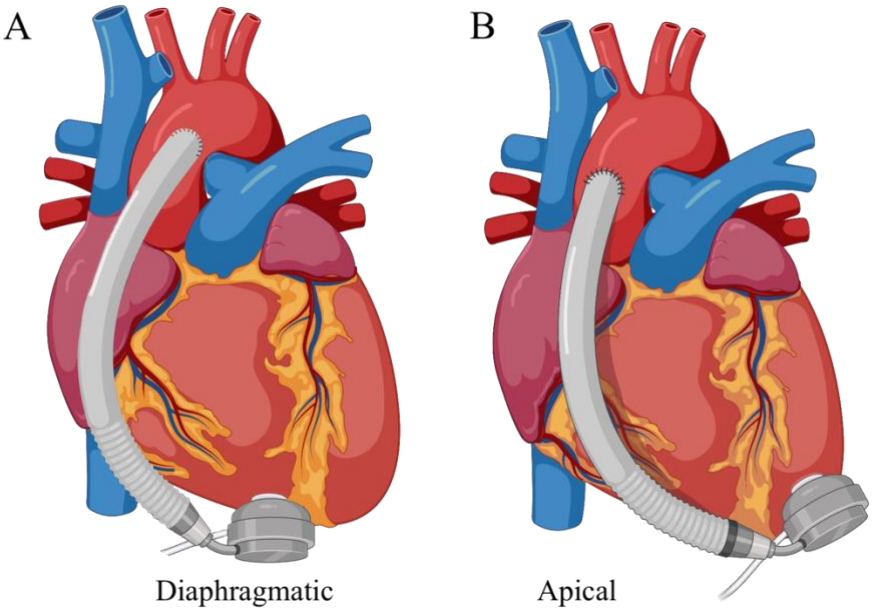

Figure 1-3: VAD Positions – The diaphragmatic (A) and apical (B) VAD inflow cannula configurations. Figure created with BioRender.com.

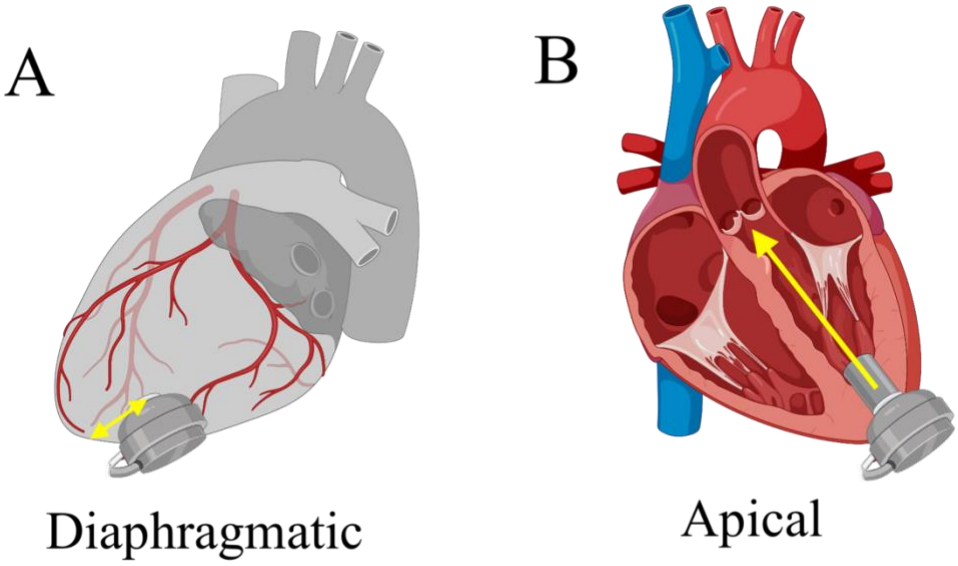

Figure 1-4: VAD Implant Procedures – The inflow cannula is placed approximately one-third from the apex of the heart at Frazier's Point (yellow arrow) when implanted on the diaphragmatic surface of the heart (A). When implanted in the apical portion of the heart, the VAD inflow cannula is aimed towards the outflow valve, parallel to the septum (yellow arrow) (B). Figure created with BioRender.com.

1.4 Ventricular Assist Device Thrombosis

Inflow cannula placement is important to consider because improper positioning can lead to complications such as thrombosis, pump exchange (costing upwards of $100,000), or even patient death [20-25]. For example, Chu et al. implanted a Berlin Heart EXCOR VAD within a four-year-old patient with HLHS. The patient survived thirteen days on VAD support before experiencing fatal complications due to pump thrombosis [26]. Unfortunately, this case is not uncommon. Buratto et al. reported that pump exchange due to thrombosis occurs in approximately 27% of post-Fontan HLHS patients [15]. Thrombosis is exacerbated due to HLHS patients' hypercoagulable state from a protein losing disorder and from pump inflow cannula malpositioning [27]. In fact, a recent study revealed that over 53% of VADs are malpositioned, and that number is estimated to be greater in pediatric patients [28]. Therefore, VAD implant inflow cannula placement needs to be optimized in order to reduce the potential for unwanted thrombus formation (Figure 1-5).

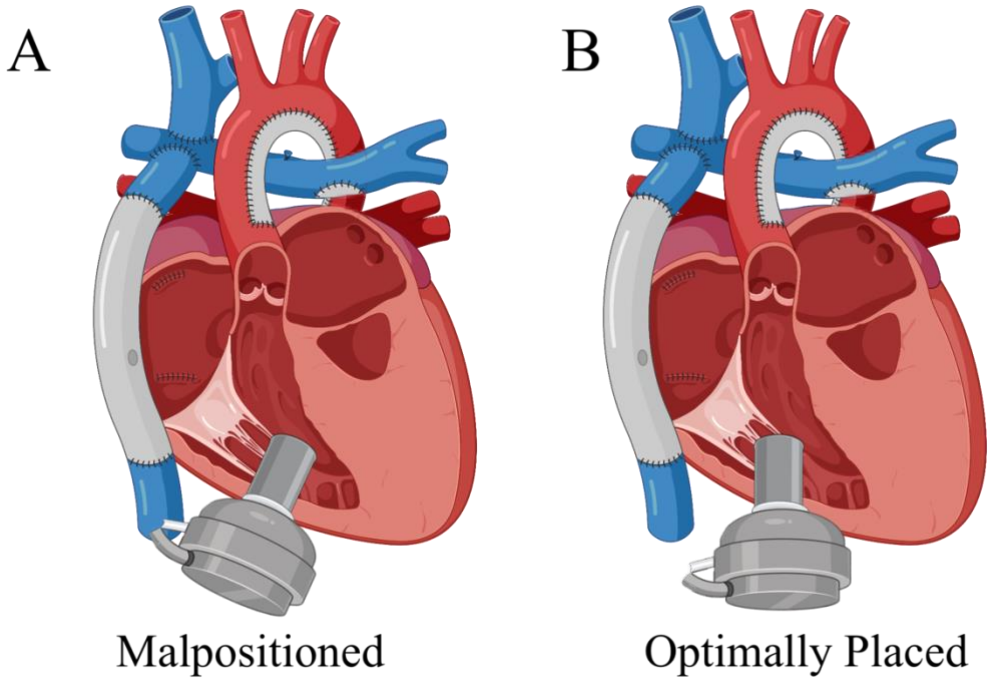

Figure 1-5: VAD Inflow Cannula Malpositioning – VAD inflow cannula positioning needs to be optimized to reduce thrombosis. A malpositioned VAD obstructs the inflow cannula (A), while a properly positioned VAD does not obstruct the inflow cannula (B). The diaphragmatic placement is shown for this example, and is hypothesized to produce properly positioned VADs when cannulas are implanted at Frazier's Point. Figure created with BioRender.com.

1.5 Aims of This Work

This work aims to investigate the relationship between ventricular assist device inflow cannula configurations and thrombus formation within single ventricle hearts. This is accomplished through a computational model and validated with a benchtop model and particle image velocimetry; the impact of this work is then highlighted through two case studies involving a novel image guided surgery platform. More specifically, Aim I utilizes a computational model to compare thrombosis risk in varying VAD implant configurations. Aim II validates the simulation results using a dynamic benchtop model and particle image velocimetry. Aim III involves the use of image guided surgery and the development of a new surgical technique for optimizing VAD implantation. Figure 1-6 provides an overview of each aim.

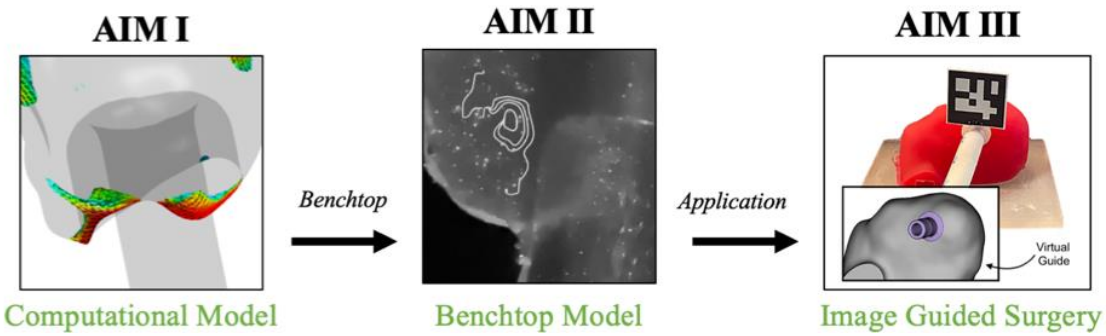

Figure 1-6: Overview of Aims – Aim I utilizes a dynamic computational model to compare thrombosis risk in VAD inflow cannula configurations. Aim II validates the simulation results using benchtop modeling and particle image velocimetry. Finally, Aim III uses a novel image guided surgery platform to optimize VAD inflow cannula positioning within single ventricle hearts.

1.6 References

[1] Siffel, C., Riehle-Colarusso, T., Oster, M. E., & Correa, A. (2015). Survival of Children With Hypoplastic Left Heart Syndrome. In Pediatrics (Vol. 136, Issue 4, pp. e864–e870). American Academy of Pediatrics (AAP). https://doi.org/10.1542/peds.2014-1427

[2] Mussa, S., & Barron, D. J. (2017). Hypoplastic left heart syndrome. In Paediatrics and Child Health (Vol. 27, Issue 2, pp. 75–82). Elsevier BV. https://doi.org/10.1016/j.paed.2016.12.002

[3] Fruitman, D. S. (2000). Hypoplastic left heart syndrome: Prognosis and management options. In Paediatrics & Child Health (Vol. 5, Issue 4, pp. 219–225). Oxford University Press (OUP). https://doi.org/10.1093/pch/5.4.219

[4] Rai, V., Gładki, M., Dudyńska, M., & Skalski, J. (2018). Hypoplastic left heart syndrome [HLHS]: treatment options in present era. In Indian Journal of Thoracic and Cardiovascular Surgery (Vol. 35, Issue 2, pp. 196–202). Springer Science and Business Media LLC. https://doi.org/10.1007/s12055-018-0742-z

[5] Griselli, M., Sinha, R., Jang, S., Perri, G., & Adachi, I. (2018). Mechanical Circulatory Support for Single Ventricle Failure. In Frontiers in Cardiovascular Medicine (Vol. 5). Frontiers Media SA. https://doi.org/10.3389/fcvm.2018.00115

[6] De Rita, F., Amodeo, A., & Hasan, A. (2017). Ventricular Assist Device Support for Hypoplastic Left Heart Syndrome, Fontan Failure, and End-Stage Systemic Right Ventricular Dysfunction. In Mechanical Circulatory Support in End-Stage Heart Failure

(pp. 381–390). Springer International Publishing. https://doi.org/10.1007/978-3-319-43383-7_38

[7] Buratto, E., Shi, W. Y., Ye, X. T., & Konstantinov, I. E. (2017). Ventricular assist devices for the failing univentricular circulation. In Expert Review of Medical Devices (Vol. 14, Issue 6, pp. 449–459). Informa UK Limited. https://doi.org/10.1080/17434440.2017.1332523

[8] Book, W. M., Gerardin, J., Saraf, A., Marie Valente, A., & Rodriguez, F., III. (2016). Clinical Phenotypes of Fontan Failure: Implications for Management. In Congenital Heart Disease (Vol. 11, Issue 4, pp. 296–308). Computers, Materials and Continua (Tech Science Press). https://doi.org/10.1111/chd.12368

[9] McCormick, A. D., & Schumacher, K. R. (2019). Transplantation of the failing Fontan. In Translational Pediatrics (Vol. 8, Issue 4, pp. 290–301). AME Publishing Company. https://doi.org/10.21037/tp.2019.06.03

[10] Jefferson, H. L., Kent, W. D. T., MacQueen, K. T., Miller, R. J. H., Holloway, D. D., & Fatehi Hassanabad, A. (2021). Left ventricular assist devices: A comprehensive review of major clinical trials, devices, and future directions. In Journal of Cardiac Surgery (Vol. 36, Issue 4, pp. 1480–1491). Wiley. https://doi.org/10.1111/jocs.15341

[11] Han, J. J., Acker, M. A., & Atluri, P. (2018). Left Ventricular Assist Devices. In Circulation (Vol. 138, Issue 24, pp. 2841–2851). Ovid Technologies (Wolters Kluwer Health). https://doi.org/10.1161/circulationaha.118.035566

[12] Timms, D. (2011). A review of clinical ventricular assist devices. In Medical Engineering & Physics (Vol. 33, Issue 9, pp. 1041–1047). Elsevier BV. https://doi.org/10.1016/j.medengphy.2011.04.010

[13] Miera, O., Potapov, E. V., Redlin, M., Stepanenko, A., Berger, F., Hetzer, R., & Hübler, M. (2011). First Experiences With the HeartWare Ventricular Assist System in Children. In The Annals of Thoracic Surgery (Vol. 91, Issue 4, pp. 1256–1260). Elsevier BV. https://doi.org/10.1016/j.athoracsur.2010.12.013

[14] Cardarelli, M. G., Salim, M., Love, J., Simone, S., Tumulty, J., Conway, D., & Griffith, B. (2009). Berlin Heart as a Bridge to Recovery for a Failing Fontan. In The Annals of Thoracic Surgery (Vol. 87, Issue 3, pp. 943–946). Elsevier BV. https://doi.org/10.1016/j.athoracsur.2008.07.086

[15] Buratto, E., Shi, W. Y., Ye, X. T., & Konstantinov, I. E. (2017). Ventricular assist devices for the failing univentricular circulation. In Expert Review of Medical Devices (Vol. 14, Issue 6, pp. 449–459). Informa UK Limited. https://doi.org/10.1080/17434440.2017.1332523

[16] Adachi, I., Burki, S., & Fraser, C. D., Jr. (2017). Current Status of Pediatric Ventricular Assist Device Support. In Seminars in Thoracic and Cardiovascular Surgery: Pediatric Cardiac Surgery Annual (Vol. 20, pp. 2–8). Elsevier BV. https://doi.org/10.1053/j.pcsu.2016.09.010

[17] Miller, J. R., Lancaster, T. S., Callahan, C., Abarbanell, A. M., & Eghtesady, P. (2018). An overview of mechanical circulatory support in single-ventricle patients. In

Translational Pediatrics (Vol. 7, Issue 2, pp. 151–161). AME Publishing Company. https://doi.org/10.21037/tp.2018.03.03

[18] Gregoric, I. D., Cohn, W. E., & Frazier, O. H. (2011). Diaphragmatic implantation of the HeartWare ventricular assist device. In The Journal of Heart and Lung Transplantation (Vol. 30, Issue 4, pp. 467–470). Elsevier BV. https://doi.org/10.1016/j.healun.2010.11.014

[19] Adamson, R. M., Mangi, A. A., Kormos, R. L., Farrar, D. J., & Dembitsky, W. P. (2014). Principles of HeartMate II Implantation to Avoid Pump Malposition and Migration. In Journal of Cardiac Surgery (Vol. 30, Issue 3, pp. 296–299). Wiley. https://doi.org/10.1111/jocs.12478

[20] Apostoli, A., Bianchi, V., Bono, N., Dimasi, A., Ammann, K. R., Moiia, Y. R., Montisci, A., Sheriff, J., Bluestein, D., Fiore, G. B., Pappalardo, F., Candiani, G., Redaelli, A., Slepian, M. J., & Consolo, F. (2019). Prothrombotic activity of cytokine-activated endothelial cells and shear-activated platelets in the setting of ventricular assist device support. In The Journal of Heart and Lung Transplantation (Vol. 38, Issue 6, pp. 658–667). Elsevier BV. https://doi.org/10.1016/j.healun.2019.02.009

[21] Scandroglio, A. M., Kaufmann, F., Pieri, M., Kretzschmar, A., Müller, M., Pergantis, P., Dreysse, S., Falk, V., Krabatsch, T., & Potapov, E. V. (2016). Diagnosis and Treatment Algorithm for Blood Flow Obstructions in Patients With Left Ventricular Assist Device. In Journal of the American College of Cardiology (Vol. 67, Issue 23, pp. 2758–2768). Elsevier BV. https://doi.org/10.1016/j.jacc.2016.03.573

[22] de Biasi, A. R., Manning, K. B., & Salemi, A. (2015). Science for surgeons: Understanding pump thrombogenesis in continuous-flow left ventricular assist devices. In The Journal of Thoracic and Cardiovascular Surgery (Vol. 149, Issue 3, pp. 667–673). Elsevier BV. https://doi.org/10.1016/j.jtcvs.2014.11.041

[23] Eckman, P. M., & John, R. (2012). Bleeding and Thrombosis in Patients With Continuous-Flow Ventricular Assist Devices. In Circulation (Vol. 125, Issue 24, pp. 3038–3047). Ovid Technologies (Wolters Kluwer Health). https://doi.org/10.1161/circulationaha.111.040246

[24] Kilic, A., Ransom, J., Maltais, S., Sun, B., Entwistle, J. W., Bailey, S., John, R., Klodell, C. T., Gregoric, I., Sheridan, B., Chuang, J., Farrar, D. J., Sundareswaran, K., & Adamson, R. (2019). Pump Position Impacts HeartMate II Left Ventricular Assist Device Thrombosis. In ASAIO Journal (Vol. 65, Issue 3, pp. 227–232). Ovid Technologies (Wolters Kluwer Health). https://doi.org/10.1097/mat.0000000000000840

[25] Baras Shreibati, J., Goldhaber-Fiebert, J. D., Banerjee, D., Owens, D. K., & Hlatky, M. A. (2017). Cost-Effectiveness of Left Ventricular Assist Devices in Ambulatory Patients With Advanced Heart Failure. In JACC: Heart Failure (Vol. 5, Issue 2, pp. 110–119). Elsevier BV. https://doi.org/10.1016/j.jchf.2016.09.008

[26] Chu, M. W. A., Sharma, K., Tchervenkov, C. I., Jutras, L. F., Lavoie, J., Shemie, S. D., Laliberte, E., Calaritis, C., & Cecere, R. (2007). Berlin Heart Ventricular Assist Device in a Child With Hypoplastic Left Heart Syndrome. In The Annals of Thoracic Surgery (Vol. 83, Issue 3, pp. 1179–1181). Elsevier BV. https://doi.org/10.1016/j.athoracsur.2006.08.020

[27] is VanderPluym, C. J., Rebeyka, I. M., Ross, D. B., & Buchholz, H. (2011). The use of ventricular assist devices in pediatric patients with univentricular hearts. In The Journal of Thoracic and Cardiovascular Surgery (Vol. 141, Issue 2, pp. 588–590). Elsevier BV. https://doi.org/10.1016/j.jtcvs.2010.06.038

[28] Sorensen, E. N., Hiivala, N. J., Jeudy, J., Rajagopal, K., & Griffith, B. P. (2013). Computed tomography correlates of inflow cannula malposition in a continuous-flow ventricular-assist device. In The Journal of Heart and Lung Transplantation (Vol. 32, Issue 6, pp. 654–657). Elsevier BV. https://doi.org/10.1016/j.healun.2013.03.010.

2. COMPUTATIONAL INVESTIGATION – AIM I

2.1. Introduction

Ventricular assist device inflow cannulas are malpositioned in over half of patients and can result in thrombus formation, pump failure, and even patient death [1-6]. Computational fluid dynamics (CFD), however, can be used to predict thrombus formation due to implantation [7-13]. CFD involves mathematically modeling physical fluid flow and solving fluid mechanics problems using numerical analysis [14]. CFD has been used extensively to evaluate VAD inflow cannula thrombosis, and a variety of computational models currently exist. Chivukula et al. developed a platelet-based thrombosis model for a left ventricular apical implant and found that thrombosis risk increased as the implant pointed away from the mitral valve [7]. Liu et al. investigated thrombosis risk in a variety of VADs using a simple Newtonian model focusing on velocity, vorticity, and wall shear stress [9]. Liao et al., on the other hand, used a more complex computational model to evaluate thrombogenic potential using strain rate criteria [12]. Sonntag et al. took a similar approach, but employed a moving mesh [15]. Most notably, Prisco et al. investigated the difference between apical and diaphragmatic inflow cannula configurations using virtual ink, and found that clearance was slightly faster for the apical placement [11].

Although these simulations have advanced the body of knowledge surrounding the relationship between VAD implant configuration and thrombosis, the studies are severely limited. For example, Chivukula et al. used a comprehensive platelet-based model, but failed to incorporate wall motion, while Sonntag et al. incorporated wall motion, but

oversimplified blood as a Newtonian fluid [7, 15]. Wall motion is important to include in a computational model as this movement affects vortex formation and flow rates [16, 17]. Furthermore, geometry should be derived from medical images such as MRI data to capture detail such as trabeculations, as these features affect flow characteristics such as strain rate [16-19]. It is also important to model blood as a non-Newtonian fluid because blood commonly exhibits this type of behavior for disease states [18]. Modeling blood as a Newtonian fluid is a common mistake in VAD simulation studies made to save simulation time, and should be avoided. Accordingly, all of the above-mentioned models have some sort of limitation and there has yet to be a comprehensive model for evaluating thrombosis risk due to VAD implantation within single ventricle hearts.

However, in order to first generate such a model, "thrombosis risk" must be defined. Virchow's triad can be used to describe thrombosis (Figure 2-1) [20]. In order for thrombus formation to occur, blood must come into contact with a non-endothelium surface; this can be the result of a tissue injury (implantation) or a foreign surface (VAD). Hypercoagulability also contributes to thrombosis risk. Patients with HLHS are more prone to clotting because of their hypercoagulable state; a protein losing enteropathy is often observed with HLHS [24]. Finally, abnormal blood flow can lead to thrombosis, and completes Virchow's triad.

Device thrombosis is primarily a platelet-mediated process [7, 25]. Regions of high shear stress activate platelets. Specifically, platelet activation occurs at shear strain rates > 2564/s [8]. The presence of the implanted inflow cannula causes recirculating low velocity, low strain rate regions to form near the device-tissue interface; this area is

commonly referred to as the "wedge region" [7]. The exact definition of "low shear strain rate" is unclear and can vary from < 250/s to < 100/s to < 2/s [8,13]. However, it is well documented that low shear strain rates contribute to platelet adhesion [8,13]. "Low velocity" required for platelet adhesion is defined as velocities < 0.001 m/s, and has been determined experimentally [13]. Finally, fluid with residence time > 5s near the implant should be considered at risk for thrombus formation [21,22]. Fluid with a low vorticity index is also considered at risk due to poor platelet washout [10,23]. It is important to note that although hemolysis is not usually factored into thrombosis risk, there is an increasing amount of evidence that suggests hemolysis can be an early predictor of thrombosis (due to the higher shear rates needed for platelet activation) [9]. A hemolysis index of > 10^{-3}% is considered at risk for thrombosis [9]. Figure 2-2 depicts thrombus formation at the device-tissue interface for a VAD inflow cannula. It is important to note that these criteria do not guarantee thrombus formation and only describe its potential; thrombosis is a complicated process that cannot be confined to a set of standard criteria [20].

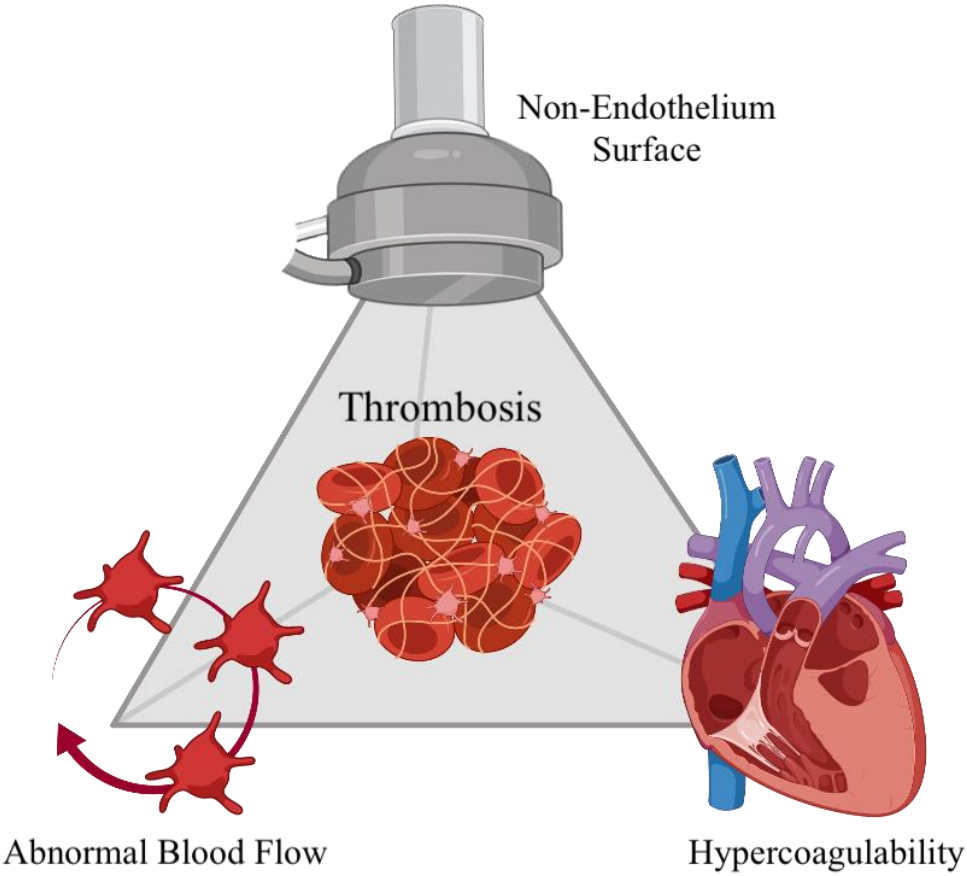

Figure 2-1: Virchow's Triad for Thrombosis – Virchow's triad for thrombosis includes contact with a non-endothelium surface, hypercoagulability, and abnormal blood flow. The VAD inflow cannula serves as a non-endothelium surface; patients with HLHS are in a hypercoagulable state due to their protein losing disorder; and VAD malpositioning leads to abnormal blood flow such as recirculating low shear regions. Figure made with BioRender.com.

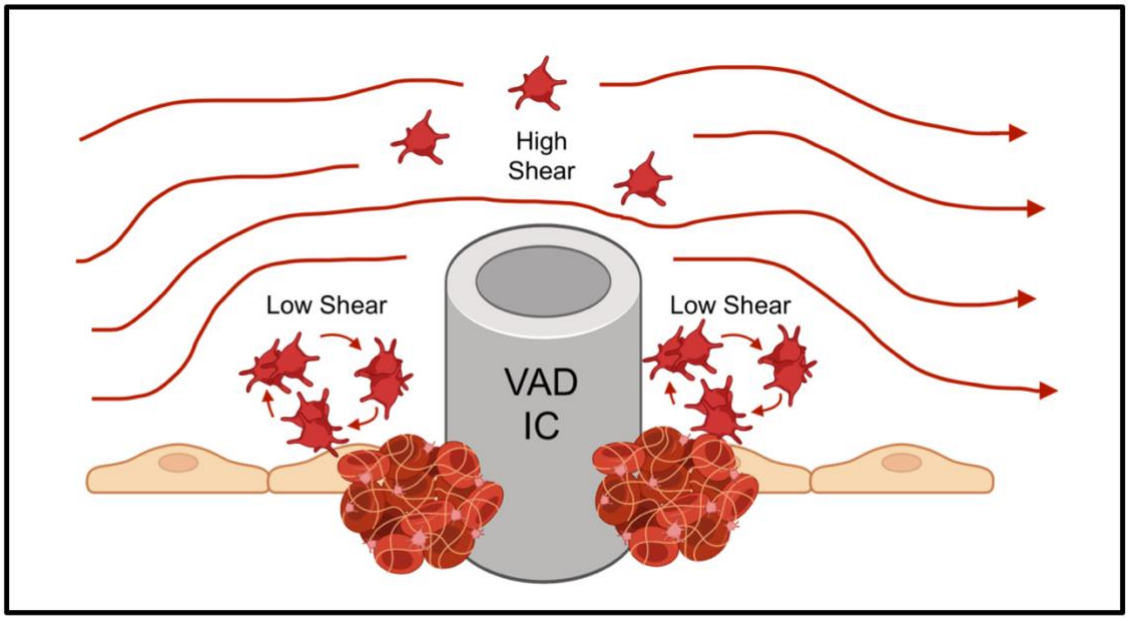

Figure 2-2: Platelet-Mediated Thrombus Formation – Thrombus formation occurs near the device-tissue interface for a VAD inflow cannula. High shear leads to platelet activation. Platelet adhesion occurs due to low velocity, low strain recirculating flow with long residence times. Poor washout and hemolysis can also contribute to thrombosis. Figure made with BioRender.com.

2.2. Methods

A 20-frame 4D MRI of a HLHS pediatric patient was obtained from the Cardiac Atlas Project [26]. Frames of the 4D MRI were registered and transforms were computed using 3D Slicer [27]. The internal blood volume at end-diastole was segmented using 3D Slicer, and a VAD inflow cannula was virtually implanted for the diaphragmatic and apical configuration into two separate volumes. The ventricular movement was generated using calculated deformable transforms, and the cannula movement was created using linear transforms from the original registered frames; this resulted in a dynamic, moving model for all phases of the cardiac cycle. Figure 2-3 illustrates the process for creating the dynamic models. An unstructured tetrahedral mesh with approximately 1.1 million elements was used to represent the cardiac geometry. This number of elements was determined from a mesh independence study (Table 2-1). There was less than a 1% difference between hemodynamic parameters of interest for the medium and fine meshes. Therefore, a 1.1 million element mesh was sufficient for simulation.

Of note, the number of elements varied slightly across each mesh due to the change in geometry. Elements had an orthogonal quality > 0.10 and a maximum skewness < 0.90, demonstrating acceptable quality for simulation. An inflation layer with a wall spacing of 0.3 mm was added to capture the velocity gradient near the wall. A laminar flow non-Newtonian Carreau model was used to simulate blood flow [17]. The details of the Carreau model are described in Table 2-2. A non-Newtonian blood model was used due to the disease state of the patient and low shears associated with platelet adhesion [17,18]. Flow was considered laminar because the Reynold's number was less than 2300 and turbulent

flow occurs when Re > 2900 for pipe flow and ventricle-like shapes [9]. The Reynold's number (Re=688) was calculated from Equation 2-1 with the values from Table 2-3 [9]. VAD flow of 3LPM was chosen to provide adequate output for this pediatric cardiac case, while preventing a suction event. An inlet velocity of 0.0811 m/s was used, and corresponded to this low flow for the large, dilated diameter of the inlet. Of note, valves were modeled as on-off orifices to reduce computational time and it was assumed that the neo-aortic valve remained closed during VAD support due to high neo-aortic pressures.

Thrombogenic potential criteria were defined by Table 2-4. The velocity and strain rate parameters were based on experimental data, as well as the residence time model that was based on the Eulerian method for convective transport of a scalar [8,13,21,22]. The hemolysis model used in this simulation employed the Eulerian method by Goubergrits et al. [28]. Fluid with high thrombosis risk satisfied the low velocity, low strain rate, and long residence time criteria defined by Table 2-4.

Table 2-1: Mesh Independence Study

Mesh Resolution	**Number of Elements**	**% Difference Between Velocity**	**% Difference Between Strain Rate**	**% Difference Between Residence Time**
Coarse Mesh	611,606	N/A	N/A	N/A
Medium Mesh	804,489	0.62%	0.25%	0.23%
Fine Mesh	1,067,486			

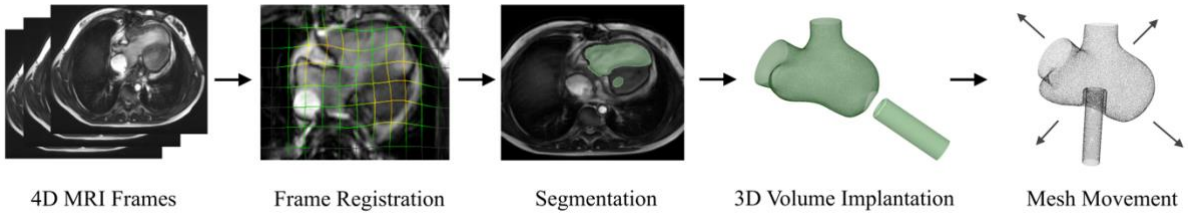

Figure 2-3: Dynamic Model Creation – 4D MRI frames are registered to each other and the transforms are computed. An initial frame is then segmented and the resulting volume is implanted with an inflow cannula. The transforms are then applied to the initial geometry to create a moving mesh.

Table 2-2: Carreau Blood Model Parameters

Parameter	**Value**
Time Constant, lambda (s)	3.313
Power-Law Index, n	0.3568
Zero Shear Viscosity (kg/ms)	0.056
Infinite Shear Viscosity (kg/ms)	0.0035
Fluid Density (kg/m^3)	1060

Equation 2-1: $\boldsymbol{Re} = \frac{\boldsymbol{\rho V D}}{\boldsymbol{\mu}}$

Table 2-3: Reynold's Number Parameters

Parameter	**Value**
Free-Stream Fluid Velocity, V (m/s)	0.0811 m/s
Characteristic Diameter, D (m)	0.028 m
Fluid density, ρ (kg/m^3)	1060
Fluid Viscosity, μ (kg/ms)	0.0035

Table 2-4: Thrombogenic Potential Criteria

Parameter	**Value**
Velocity	< 0.001 m/s
Shear Strain Rate (Platelet Adhesion)	< 250/s (or < 2/s)
Shear Strain Rate (Platelet Activation)	> 2564/s
Residence Time	> 5s
Hemolysis Index	> 1×10^{-3} %

2.3. Results

The diaphragmatic and apical configurations both exhibited regions of potential thrombosis risk near the implantation site (Figure 2-4A vs. Figure 2-4B); however, there was an average greater volume of fluid with thrombogenic potential in the apical placement (Figure 2-5). The average velocity and strain rates for fluid satisfying thrombosis risk criteria were similar for both implant configurations. Average residence times varied greatly per implant positions. The average residence time for fluid at risk for thrombus formation in the diaphragmatic configuration was 16.4 seconds (Figure 2-5). The average residence time for fluid at risk for thrombus formation in the apical configuration was greater at 21.49 seconds (Figure 2-5). Additionally, upon visual inspection, the apical implant configuration featured a greater amount of fluid with high residence times near the implant site (Figure 2-4H).

The diaphragmatic configuration exhibited a high average vorticity index of 22.69/s, while the apical configuration had a much lower value of 9.3/s (Figure 2-5). There was also a noticeable difference between hemolysis indices for the two implant positions. The apical configuration featured more than double hemolysis in at-risk regions in comparison to the diaphragmatic configuration (Figure 2-5). Of note, neither value met the criteria for critical blood damage and potential thrombus formation due to hemolysis.

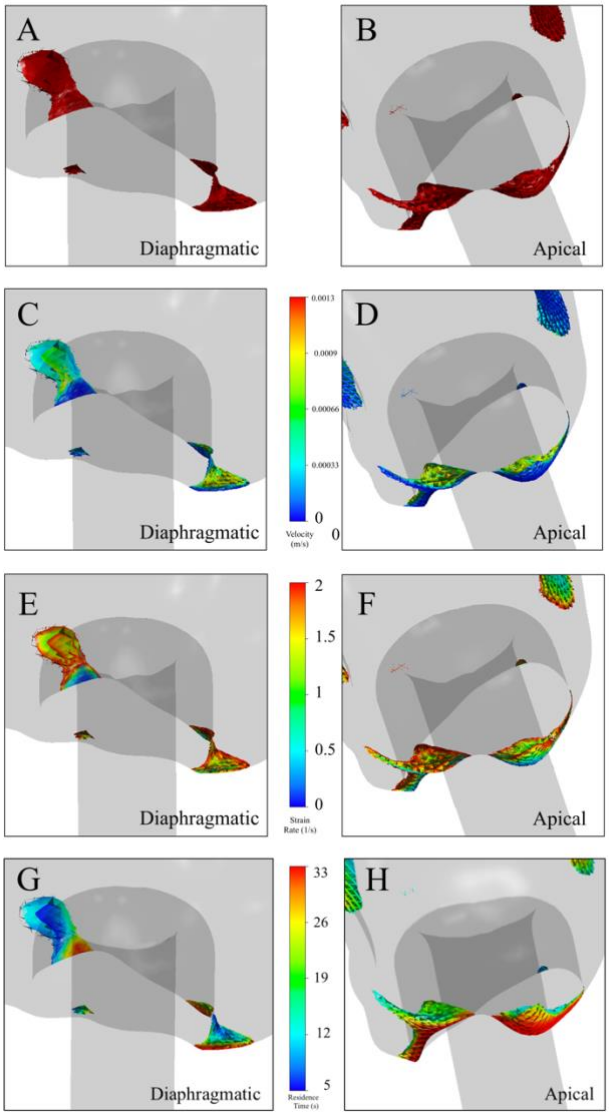

Figure 2-4: CFD Results – The diaphragmatic (A) and apical (B) configurations both featured volumes of fluid at risk of thrombus formation. The diaphragmatic and apical positions had similar velocities (C vs. D) and strain rates (E vs. F), respectively. The diaphragmatic configuration had shorter residence times in comparison to the apical configuration (G vs. H).

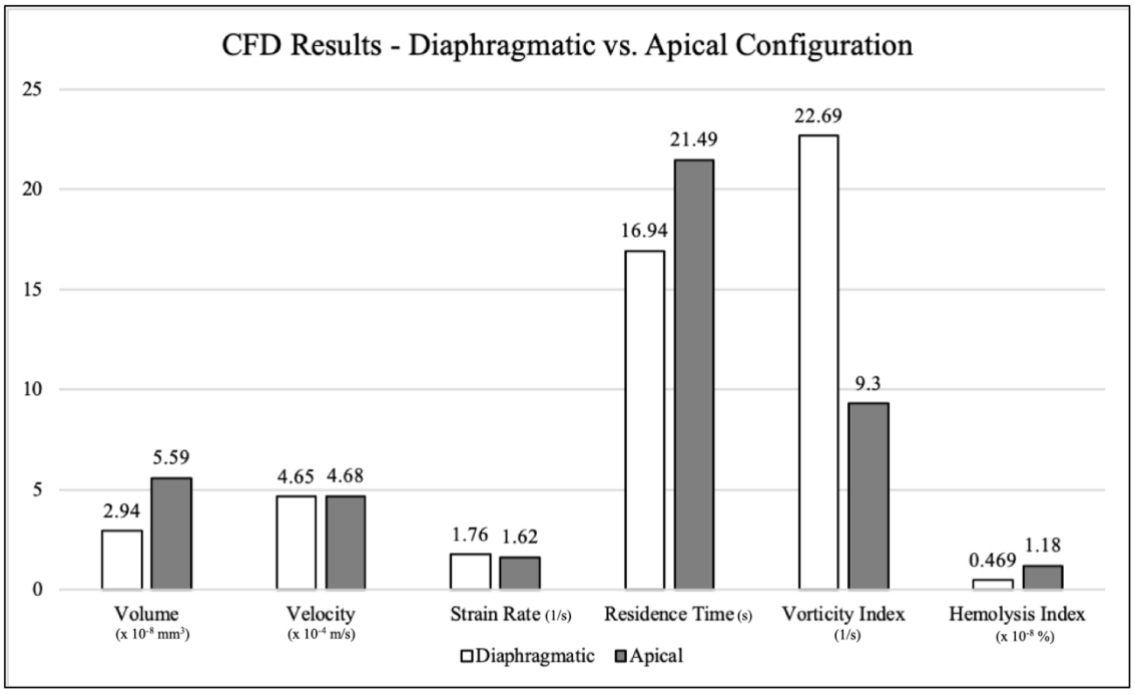

Figure 2-5: Comparison of Values from CFD Study – The apical configuration had a greater volume of fluid at risk for thrombus formation than the diaphragmatic configuration. The two implant positions produced similar velocities and strain rates in at-risk fluid regions. The apical configuration had longer residence times, a lower vorticity index (poor washout), and higher hemolysis index.

2.4. Discussion

Although there was an observable difference in thrombosis risk for the apical vs. diaphragmatic implant configurations, several limitations exist that should be considered. Valves were modeled as on-off orifices to save computational time. Although this was a valid assumption, valve motion can contribute to the development of important flow patterns and vortices within the fluid domain, and should be included for completeness [17]. The dynamic mesh was also limited by the 20 frames of the MRI as results were interpolated across meshes. Ideally, there should be finer resolution between meshes to improve the accuracy of results.

Furthermore, only one case was investigated, featuring a patient-specific geometry and ventricular shape. More cases should be explored to draw a definitive conclusion regarding the relationship between VAD inflow cannula configuration and thrombus formation. However, it is clear that an unobstructed inflow cannula leads to reduced thrombosis risk. For this case, the diaphragmatic implant configuration allows more space around the implant, leading to a less obstructed inflow cannula – especially as the heart wall deforms. The walls of the heart potentially impinge upon the inflow when in motion for the apical case for a patient with HLHS ventricular geometry (Figure 2-6). It is important to note that this may not be true for another congenital anomaly and is specific to HLHS.

Additionally, simulation results should never supersede years of surgeon experience, and should only serve as a reference with many caveats. Thrombosis is a complicated process as evidenced by Virchow's Triad and the coagulation cascade, and

virtual surgery cannot capture the minutiae of physical surgery (such as the surgical logistics of implanting a VAD within a small patient chest cavity) [20]. It is also interesting to consider the effect of remodeling of the heart on the inflow cannula position. Studies have shown that inflow cannula position changes as the heart remodels [7]. Even though HLHS patients are on short-term VAD support, remodeling must be considered. To solve this problem, May-Newman et al. have proposed a "tipless" cannula design flush with the implant site to minimize the effect of VAD malpositioning; however, the technology is in early development [29]. Regardless, a centrally placed VAD with an unobstructed inflow cannula can reduce thrombosis risk and the potential for malpositioning as the heart remodels over time.

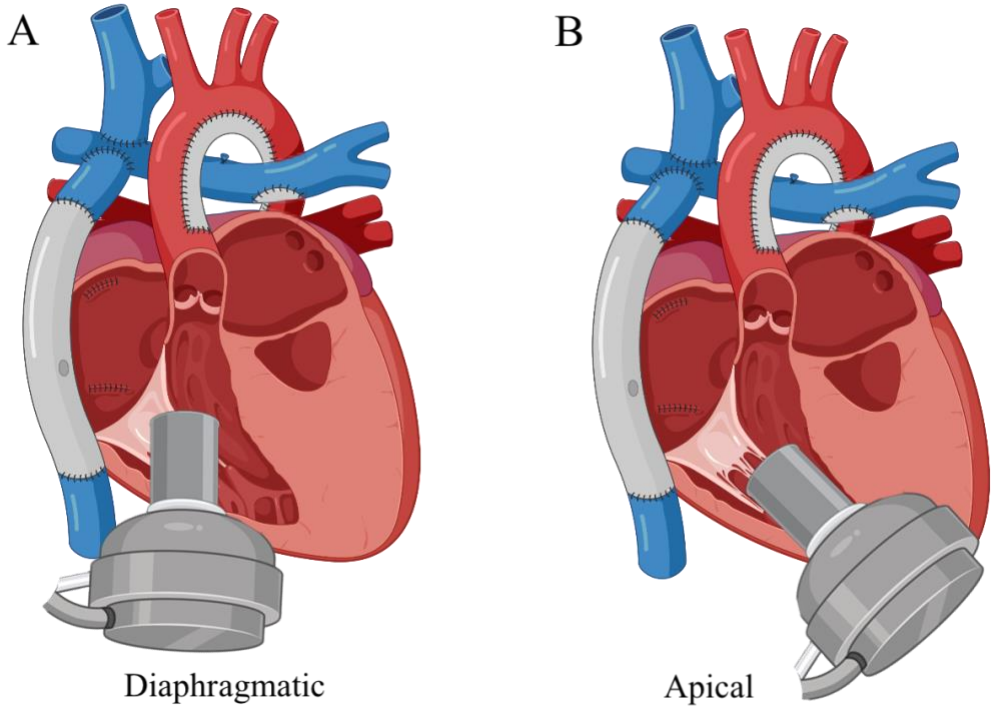

Figure 2-6: The Diaphragmatic vs. Apical Position – When a VAD is placed in the diaphragmatic configuration (A), it has more three-dimensional space within the single systemic ventricle. Therefore, the inflow cannula is less obstructed – especially as the wall deforms throughout the cardiac cycle. When a VAD is placed in the apical configuration (B), it has less space within the single systemic ventricle and can become obstructed by the dense trabeculations. Figure made with BioRender.com

2.5. References

[1] Sorensen, E. N., Hiivala, N. J., Jeudy, J., Rajagopal, K., & Griffith, B. P. (2013). Computed tomography correlates of inflow cannula malposition in a continuous-flow ventricular-assist device. In The Journal of Heart and Lung Transplantation (Vol. 32, Issue 6, pp. 654–657). Elsevier BV. https://doi.org/10.1016/j.healun.2013.03.010.

[2] Apostoli, A., Bianchi, V., Bono, N., Dimasi, A., Ammann, K. R., Moiia, Y. R., Montisci, A., Sheriff, J., Bluestein, D., Fiore, G. B., Pappalardo, F., Candiani, G., Redaelli, A., Slepian, M. J., & Consolo, F. (2019). Prothrombotic activity of cytokine-activated endothelial cells and shear-activated platelets in the setting of ventricular assist device support. In The Journal of Heart and Lung Transplantation (Vol. 38, Issue 6, pp. 658–667). Elsevier BV. https://doi.org/10.1016/j.healun.2019.02.009

[3] Scandroglio, A. M., Kaufmann, F., Pieri, M., Kretzschmar, A., Müller, M., Pergantis, P., Dreysse, S., Falk, V., Krabatsch, T., & Potapov, E. V. (2016). Diagnosis and Treatment Algorithm for Blood Flow Obstructions in Patients With Left Ventricular Assist Device. In Journal of the American College of Cardiology (Vol. 67, Issue 23, pp. 2758–2768). Elsevier BV. https://doi.org/10.1016/j.jacc.2016.03.573

[4] de Biasi, A. R., Manning, K. B., & Salemi, A. (2015). Science for surgeons: Understanding pump thrombogenesis in continuous-flow left ventricular assist devices. In The Journal of Thoracic and Cardiovascular Surgery (Vol. 149, Issue 3, pp. 667–673). Elsevier BV. https://doi.org/10.1016/j.jtcvs.2014.11.041

[5] Eckman, P. M., & John, R. (2012). Bleeding and Thrombosis in Patients With Continuous-Flow Ventricular Assist Devices. In Circulation (Vol. 125, Issue 24, pp.

3038–3047). Ovid Technologies (Wolters Kluwer Health). https://doi.org/10.1161/circulationaha.111.040246

[6] Kilic, A., Ransom, J., Maltais, S., Sun, B., Entwistle, J. W., Bailey, S., John, R., Klodell, C. T., Gregoric, I., Sheridan, B., Chuang, J., Farrar, D. J., Sundareswaran, K., & Adamson, R. (2019). Pump Position Impacts HeartMate II Left Ventricular Assist Device Thrombosis. In ASAIO Journal (Vol. 65, Issue 3, pp. 227–232). Ovid Technologies (Wolters Kluwer Health). https://doi.org/10.1097/mat.0000000000000840

[7] Chivukula, V. K., Beckman, J. A., Prisco, A. R., Dardas, T., Lin, S., Smith, J. W., Mokadam, N. A., Aliseda, A., & Mahr, C. (2018). Left Ventricular Assist Device Inflow Cannula Angle and Thrombosis Risk. In Circulation: Heart Failure (Vol. 11, Issue 4). Ovid Technologies (Wolters Kluwer Health). https://doi.org/10.1161/circheartfailure.117.004325

[8] Fraser, K. H., Zhang, T., Taskin, M. E., Griffith, B. P., & Wu, Z. J. (2010). Computational Fluid Dynamics Analysis of Thrombosis Potential in Left Ventricular Assist Device Drainage Cannulae. In ASAIO Journal (Vol. 56, Issue 3, pp. 157–163). Ovid Technologies (Wolters Kluwer Health). https://doi.org/10.1097/mat.0b013e3181d861f1

[9] Liu, G.-M., Chen, H.-B., Luo, F.-L., Zhang, Y., Sun, H.-S., Zhou, J.-Y., & Hu, S.-S. (2012). Numerical Simulation of LVAD Inflow Cannulas with Different Tip. In International Journal of Chemical Engineering (Vol. 2012, pp. 1–8). Hindawi Limited. https://doi.org/10.1155/2012/596960

[10] Ong, C., Dokos, S., Chan, B., Lim, E., Abed, A. A., Osman, N., Kadiman, S., & Lovell, N. H. (2013). Numerical investigation of the effect of cannula placement on thrombosis. In Theoretical Biology and Medical Modelling (Vol. 10, Issue 1). Springer Science and Business Media LLC. https://doi.org/10.1186/1742-4682-10-35

[11] Prisco, A. R., Aliseda, A., Beckman, J. A., Mokadam, N. A., Mahr, C., & Garcia, G. J. M. (2017). Impact of LVAD Implantation Site on Ventricular Blood Stagnation. In ASAIO Journal (Vol. 63, Issue 4, pp. 392–400). Ovid Technologies (Wolters Kluwer Health). https://doi.org/10.1097/mat.0000000000000503

[12] Liao, S., Neidlin, M., Li, Z., Simpson, B., & Gregory, S. D. (2018). Ventricular flow dynamics with varying LVAD inflow cannula lengths: In-silico evaluation in a multiscale model. In Journal of Biomechanics (Vol. 72, pp. 106–115). Elsevier BV. https://doi.org/10.1016/j.jbiomech.2018.02.038

[13] Liao, S., Simpson, B., Neidlin, M., Kaufmann, T. A. S., Li, Z., Woodruff, M. A., & Gregory, S. D. (2016). Numerical prediction of thrombus risk in an anatomically dilated left ventricle: the effect of inflow cannula designs. In BioMedical Engineering OnLine (Vol. 15, Issue S2). Springer Science and Business Media LLC. https://doi.org/10.1186/s12938-016-0262-2

[14] Tryggvason, G. (2016). Computational Fluid Dynamics. In Fluid Mechanics (pp. 227–291). Elsevier. https://doi.org/10.1016/b978-0-12-405935-1.00006-x

[15] Sonntag, S. J., Lipinski, E., Neidlin, M., Hugenroth, K., Benkowski, R., Motomura, T., & Kaufmann, T. A. S. (2019). Virtual Fitting and Hemodynamic Simulation of the EVAHEART 2 Left Ventricular Assist Device and Double-Cuff Tipless Inflow Cannula.

In ASAIO Journal (Vol. 65, Issue 7, pp. 698–706). Ovid Technologies (Wolters Kluwer Health). https://doi.org/10.1097/mat.0000000000000867

[16] Chnafa, C., Mendez, S., & Nicoud, F. (2016). Image-Based Simulations Show Important Flow Fluctuations in a Normal Left Ventricle: What Could be the Implications? In Annals of Biomedical Engineering (Vol. 44, Issue 11, pp. 3346–3358). Springer Science and Business Media LLC. https://doi.org/10.1007/s10439-016-1614-6

[17] Doost, S. N., Ghista, D., Su, B., Zhong, L., & Morsi, Y. S. (2016). Heart blood flow simulation: a perspective review. In BioMedical Engineering OnLine (Vol. 15, Issue 1). Springer Science and Business Media LLC. https://doi.org/10.1186/s12938-016-0224-8

[18] Doost, S. N., Zhong, L., Su, B., & Morsi, Y. S. (2016). The numerical analysis of non-Newtonian blood flow in human patient-specific left ventricle. In Computer Methods and Programs in Biomedicine (Vol. 127, pp. 232–247). Elsevier BV. https://doi.org/10.1016/j.cmpb.2015.12.020

[19] Sacco, F., Paun, B., Lehmkuhl, O., Iles, T. L., Iaizzo, P. A., Houzeaux, G., Vázquez, M., Butakoff, C., & Aguado-Sierra, J. (2018). Left Ventricular Trabeculations Decrease the Wall Shear Stress and Increase the Intra-Ventricular Pressure Drop in CFD Simulations. In Frontiers in Physiology (Vol. 9). Frontiers Media SA. https://doi.org/10.3389/fphys.2018.00458

[20] Patravale, V., Dandekar, P., & Jain, R. (2012). Characterization techniques for nanoparticulate carriers. In Nanoparticulate Drug Delivery (pp. 87–121). Elsevier. https://doi.org/10.1533/9781908818195.87

[21] Sarrami-Foroushani, A., Lassila, T., Hejazi, S. M., Nagaraja, S., Bacon, A., & Frangi, A. F. (2019). A computational model for prediction of clot platelet content in flow-diverted intracranial aneurysms. In Journal of Biomechanics (Vol. 91, pp. 7–13). Elsevier BV. https://doi.org/10.1016/j.jbiomech.2019.04.045

[22] Rayz, V. L., Boussel, L., Ge, L., Leach, J. R., Martin, A. J., Lawton, M. T., McCulloch, C., & Saloner, D. (2010). Flow Residence Time and Regions of Intraluminal Thrombus Deposition in Intracranial Aneurysms. In Annals of Biomedical Engineering (Vol. 38, Issue 10, pp. 3058–3069). Springer Science and Business Media LLC. https://doi.org/10.1007/s10439-010-0065-8

[23] Laumen, M., Kaufmann, T., Timms, D., Schlanstein, P., Jansen, S., Gregory, S., Wong, K. C., Schmitz-Rode, T., & Steinseifer, U. (2010). Flow Analysis of Ventricular Assist Device Inflow and Outflow Cannula Positioning Using a Naturally Shaped Ventricle and Aortic Branch. In Artificial Organs (Vol. 34, Issue 10, pp. 798–806). Wiley. https://doi.org/10.1111/j.1525-1594.2010.01098.x

[24] McCormick, A. D., & Schumacher, K. R. (2019). Transplantation of the failing Fontan. In Translational Pediatrics (Vol. 8, Issue 4, pp. 290–301). AME Publishing Company. https://doi.org/10.21037/tp.2019.06.03

[25] Apostoli, A., Bianchi, V., Bono, N., Dimasi, A., Ammann, K. R., Moiia, Y. R., Montisci, A., Sheriff, J., Bluestein, D., Fiore, G. B., Pappalardo, F., Candiani, G., Redaelli, A., Slepian, M. J., & Consolo, F. (2019). Prothrombotic activity of cytokine-activated endothelial cells and shear-activated platelets in the setting of ventricular assist device

support. In The Journal of Heart and Lung Transplantation (Vol. 38, Issue 6, pp. 658–667). Elsevier BV. https://doi.org/10.1016/j.healun.2019.02.009

[26] Fonseca, C. G., Backhaus, M., Bluemke, D. A., Britten, R. D., Chung, J. D., Cowan, B. R., Dinov, I. D., Finn, J. P., Hunter, P. J., Kadish, A. H., Lee, D. C., Lima, J. A. C., Medrano−Gracia, P., Shivkumar, K., Suinesiaputra, A., Tao, W., & Young, A. A. (2011). The Cardiac Atlas Project—an imaging database for computational modeling and statistical atlases of the heart. In Bioinformatics (Vol. 27, Issue 16, pp. 2288–2295). Oxford University Press (OUP). https://doi.org/10.1093/bioinformatics/btr360

[27] Fedorov, A., Beichel, R., Kalpathy-Cramer, J., Finet, J., Fillion-Robin, J.-C., Pujol, S., Bauer, C., Jennings, D., Fennessy, F., Sonka, M., Buatti, J., Aylward, S., Miller, J. V., Pieper, S., & Kikinis, R. (2012). 3D Slicer as an image computing platform for the Quantitative Imaging Network. In Magnetic Resonance Imaging (Vol. 30, Issue 9, pp. 1323–1341). Elsevier BV. https://doi.org/10.1016/j.mri.2012.05.001

[28] Goubergrits, L., & Affeld, K. (2004). Numerical Estimation of Blood Damage in Artificial Organs. In Artificial Organs (Vol. 28, Issue 5, pp. 499–507). Wiley. https://doi.org/10.1111/j.1525-1594.2004.07265.x

[29] May-Newman, K., Montes, R., Campos, J., Marquez-Maya, N., Vu, V., Zebrowski, E., Motomura, T., & Benkowski, R. (2019). Reducing regional flow stasis and improving intraventricular hemodynamics with a tipless inflow cannula design: An in vitro flow visualization study using the EVAHEART LVAD. In Artificial Organs (Vol. 43, Issue 9, pp. 834–848). Wiley. https://doi.org/10.1111/aor.13477

3. BENCHTOP VALIDATION – AIM II

3.1. Introduction

Several research institutions in conjunction with the FDA have recently released a series of studies comparing computational and experimental results to make a statement on the reliability of CFD and need for validation of computational results. For example, Morrison et al. proposed best practices for assessing blood pump hemolysis *in silico* and discussed the risks associated with CFD models [1]. Malinauskas et al. demonstrated the differences in computational and benchtop data for nozzle and blood pump devices, with emphasis on the importance of validating CFD studies [2]. Often, *in silico* and experimental results can vary by orders of magnitude [1,2]. Therefore, computational models must be validated with benchtop studies in order to provide meaningful and reliable results.

Mock circulation loops (MCLs) are commonly used to validate computational studies involving ventricular assist device implants [3]. MCLs are also known as "ventricular benchtop models" or "pulse duplicators," and can be fine-tuned to mechanically represent the cardiac circulatory system [3]. MCLs typically consist of a fluid reservoir, pump, compliance chamber, and resistance element [3]. Additional components such as valves, flow meters, and pressure catheters are often included. The arterial system is usually modeled as a Windkessel with the compliance chamber simulating the elastic arteries and a downstream clamp providing peripheral resistance (Figure 3-1) [4]. Of note, a fluid reservoir open to air provides preload to the heart.

MCLs have evolved significantly over the years. Pantalos et al. gained recognition with their four-chamber MCL for VAD testing [5]. Giridharan et al. created a novel MCL to investigate VAD flow within failing Fontan pediatric patients [6]. May-Newman et al. have provided one of the most interesting innovations to MCL design with their deformable ventricular sac inside a pressure chamber [7,8]. Accordingly, as the pressure in the tank changes, the sac deforms, mimicking the pumping action of the heart. Many other research groups have adopted this clever design, and it has become a standard component in MCLs [9-11]. However, the ventricular sacs in many of these studies are idealized [5-11]. It is important to include patient-specific geometry such as dense trabeculations because these details can alter fluid flow and vortex patterns [12,13]. May-Newman et al. have also popularized the use of particle image velocimetry (PIV) with MCL testing [7,8]. PIV is an optical method for flow visualization used to obtain instantaneous velocity measurements and other related properties (such as shear strain rate) [14]. PIV systems are expensive, costing upwards of $100,000 per unit, and are therefore not easily accessible to researchers, limiting the number of PIV studies that can be performed in conjunction with other benchtop experiments [15,16]. Accordingly, the current process for validating CFD is limited, and could be improved. A patient-specific deformable sac MCL is therefore presented and analyzed using a low-cost particle image velocimetry system.

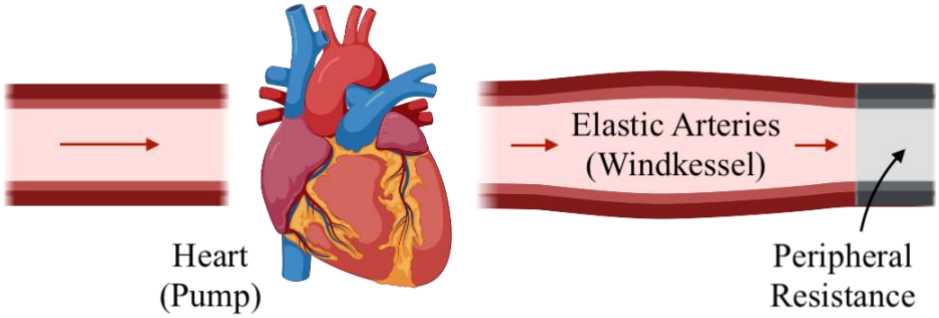

Figure 3-1: The Windkessel Model – The elastic arteries act as a "Windkessel" or compliance chamber in the system. Figure made with BioRender.com.

3.2. Methods

The proposed mock circulatory loop consisted of a deformable ventricular sac surrounded by an acrylic pumping chamber filled with fluid. The circulating fluid was a blood analogue composed of 60% water and 40% glycerin to mimic the fluid and optical properties needed for analysis [23]. The MCL also featured a filling reservoir for preload, compliance chamber to model elastic arteries, adjustable valve for peripheral resistance, and several one-way flow valves to represent physiological valves (Figure 3-2 and Figure 3-3) [22]. Pressure was measured with Camino Integra pressure catheters, and flow was measured with several flow meters (Great Plain Industrials TM Series and IFM SM6100) (Figure 3-3).

The geometry for the ventricular sac was obtained from a post-Fontan HLHS MRI from the Cardiac Atlas Project [17]. The internal blood volume for end-diastole was segmented using 3D Slicer [18]. Cannulas were implanted virtually in the diaphragmatic

and apical configurations and each volume was 3D printed [19,20]. Three layers of Smooth-On SORTA-CLEAR 37 were painted on each 3D printed volume with an average final layer thickness of 1.48 +/- 0.22 mm (Figure 3-4). This material was chosen due to its "water-clear translucent optical properties" and ability to closely match the refractive indices of the working fluids [21]. Of note, the silicone was also compliance-matched to the heart according to Equation 3-1 and the values in Table 3-1 [24]. A wall thickness of approximately 1.42 mm was used to achieve compliance matching.

Pre-VAD and VAD conditions were modeled according to Table 3-2. An EDP > 15 mmHg signified systolic failure for this HLHS case [6,9]. Target flow was 2.0 LPM with 90 BPM for heart failure conditions [6,9]. VAD support aimed to increase flow while decreasing EDP between 3 mmHg and 15 mmHg [6]. A low-cost PIV system was used to analyze flow. The platform consisted of a 532 nm laser, an iPhone 7 with autofocus disabled, and microballoons as the tracking particles [15,16]. 2D planar PIV was employed and slow-motion video was used for acquisition. PIVLab MATLAB was used to analyze results [25].

Equation 3-1: $\boldsymbol{C = \frac{2\pi r^3}{A_{min} E h}}$

Table 3-1: Compliance Matching

Parameter	**Cardiac Tissue**	**Silicone Sac**
Radius, r (m)	0.011	0.014
Minimum Area, A_{min} (m^2)	0.0003801	0.0006246
Young's Modulus, E (Pa)	0.526×10^6	0.621×10^6
Wall thickness, h (m)	0.00132	0.00142
Compliance, C (1/Pa)	31.25×10^{-6}	31.25×10^{-6}

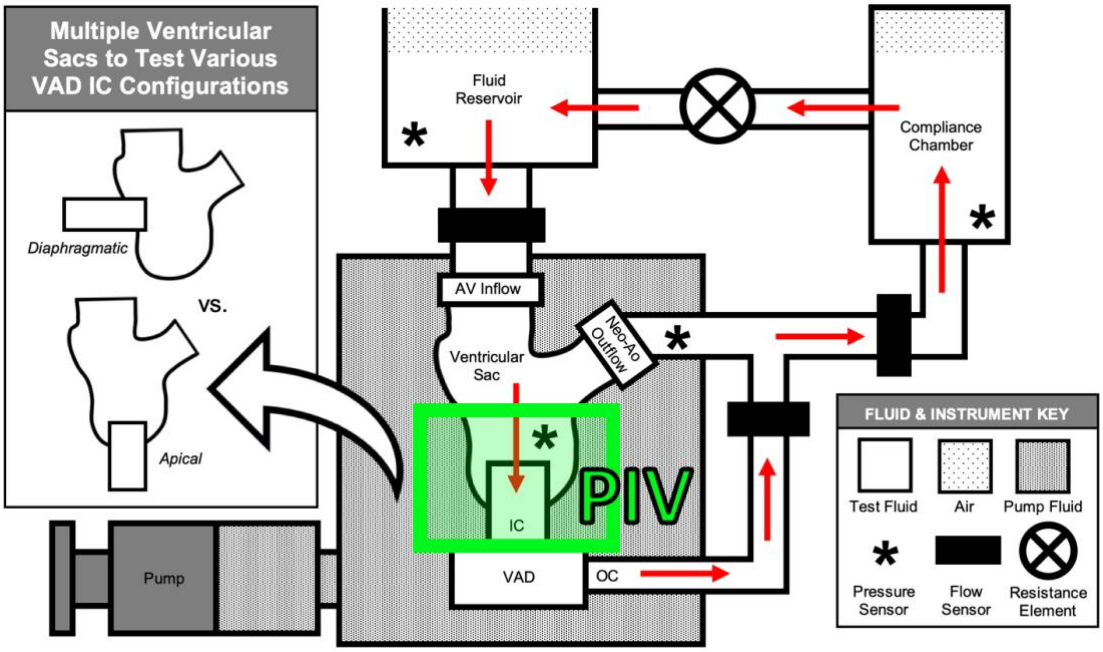

Figure 3-2: Mock Circulatory Loop Schematic – The proposed MCL consists of a fluid reservoir, deformable ventricular sac inside a pressure tank, compliance chamber, and resistance element. Pressure catheters and flow meters provide measurements. The diaphragmatic and apical configurations can be tested and analyzed using particle image velocimetry (PIV).

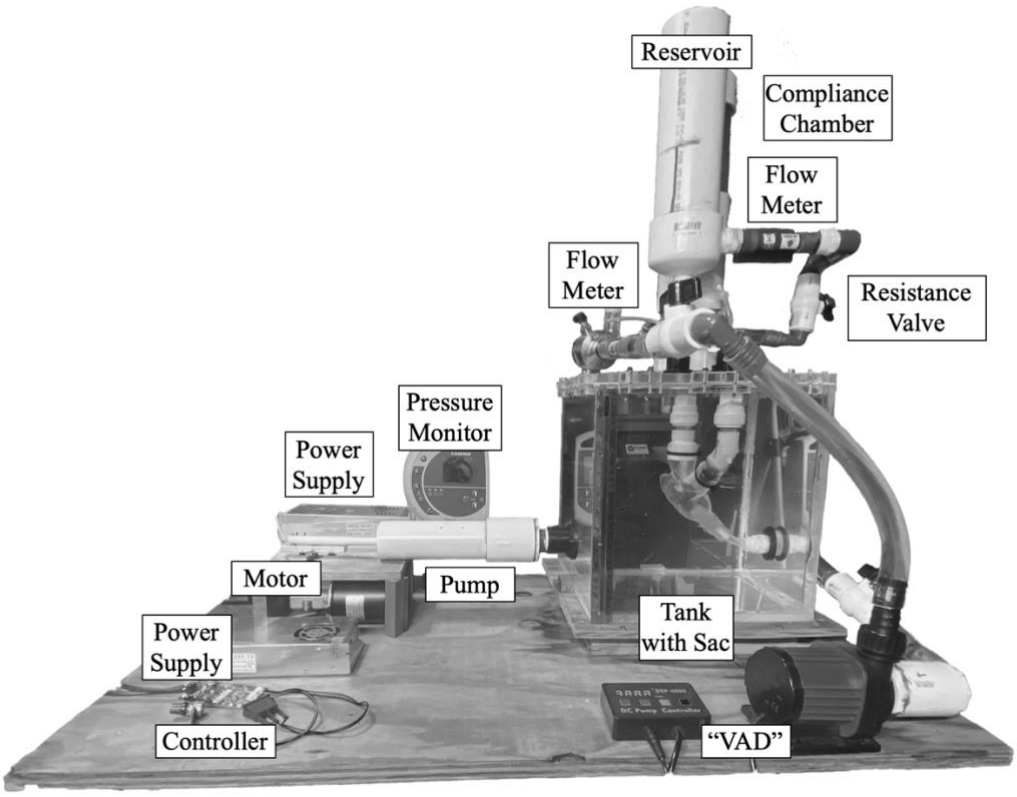

Figure 3-3: Mock Circulatory Loop Components – The MCL consists of a fluid reservoir, deformable ventricular sac inside a pressure tank, compliance chamber, and resistance element. A pump can be turned on to simulate VAD flow.

Figure 3-4: The Optically Clear Deformable Sac – The optically-clear silicone ventricular sac features dense trabeculations specific to the HLHS patient.

Table 3-2: Mock Circulatory Loop Target Parameters

Parameter	**Pre-VAD Support**	**VAD Support**
End Diastolic Pressure, EDP (mmHg)	> 15	> 3, <15
Peak Systolic Ventricular Pressure, SVP (mmHg)	70	< 70
Peak Systolic neo-Aortic Pressure, neo-AoP (mmHg)	65	>65
Flow, Liters per Minute (LPM)	2.0	> 2.0

3.3. Results

The mock circulation loop was able to simulate pre-VAD support and VAD support conditions as expected (Table 3-3). The end diastolic ventricular pressure prior to VAD support was 19.6 +/- 0.2 mmHg. After VAD support, this value decreased to 7.5 +/- 0.3 mmHg. Flow also increased with VAD support from 2.0 +/- 0.3 LPM to 3.1 +/- 0.4 LPM (Figure 3-5). VAD flow could not be increased without inducing suction events. As expected with VAD support, neo-aortic pressure also increased from 64.4 +/- 8.8 mmHg to 89.3 +/- 6.1 mmHg. Of note, due to high neo-aortic pressures, the neo-aortic valve remained closed during VAD support.

Particle image velocimetry was successfully completed using the low-cost imaging system (Figure 3-6). PIV revealed low velocity, low strain rate recirculating flow in both the apical and diaphragmatic configurations near the implant site (Figure 3-7). However, the apical configuration produced increased regions of low velocity low strain flow; this trend was also observed computationally (Figure 3-8). It is important to note that while PIV confirmed CFD trends, individual numbers varied, with CFD results being consistently higher in magnitude.

Table 3-3: Mock Circulatory Loop Results

Parameter	**Pre-VAD**	**Post-VAD**	**Change**
EDVP (mmHg)	19.6 +/- 0.2	7.5 +/- 0.3	62% decrease
Peak SVP (mmHg)	71.2 +/- 10.0	53.1 +/- 10.9	25% decrease
Peak Systolic neo-AoP (mmHg)	64.4 +/- 8.8	89.3 +/- 6.1	39% increase
Flow (LPM)	2.0 +/- 0.3	3.1 +/- 0.4	55% increase

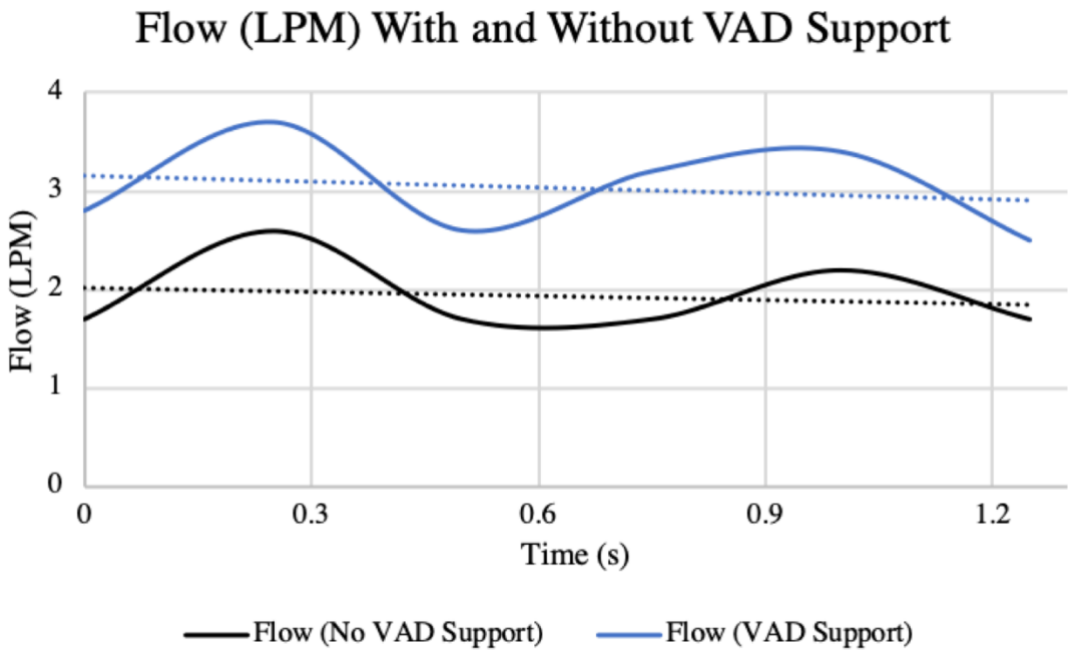

Figure 3-5: Mock Circulatory Loop Flow Data – Flow increased from about 2.0 LPM to 3.1 LPM with VAD support.

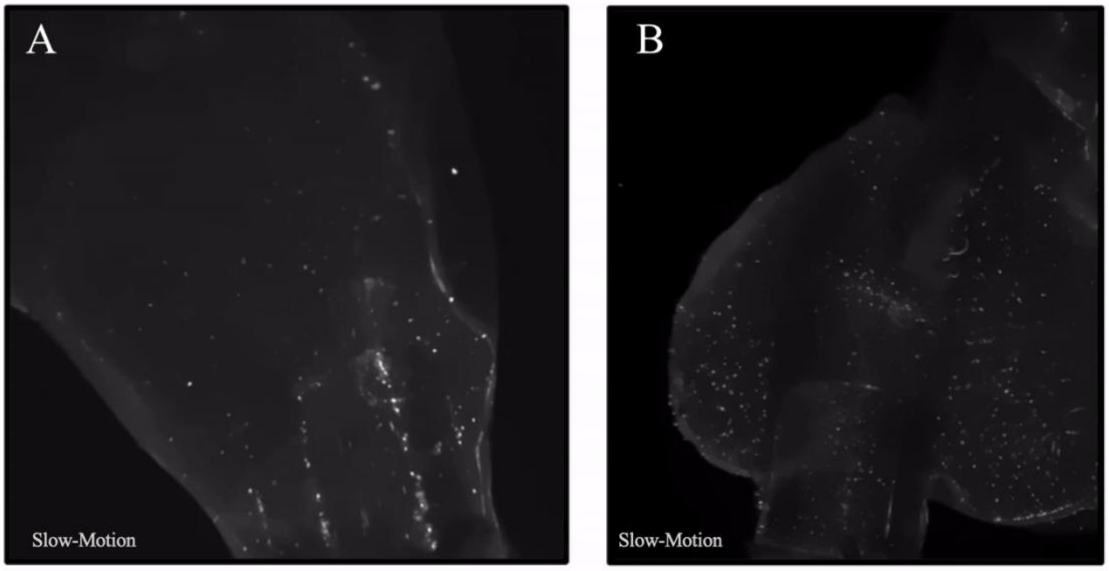

Figure 3-6: Particle Image Velocimetry Frames – The low-cost PIV system successfully tracked particles within the apical (A) and diaphragmatic (B) configurations.

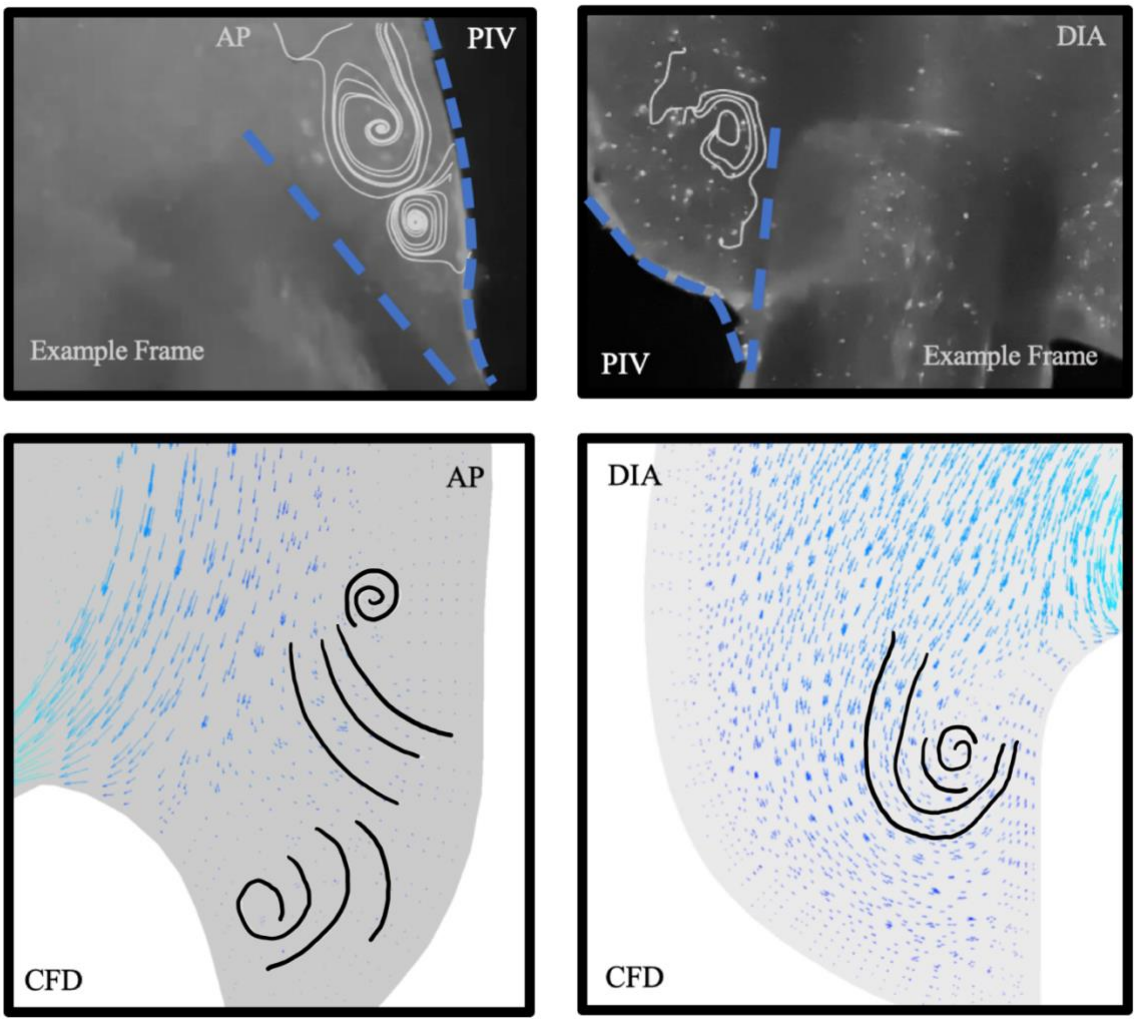

Figure 3-7: PIV vs. CFD Comparison – Recirculating flow regions matched for PIV and CFD cases for the apical (left panel) and diaphragmatic (right panel) cases, respectively.

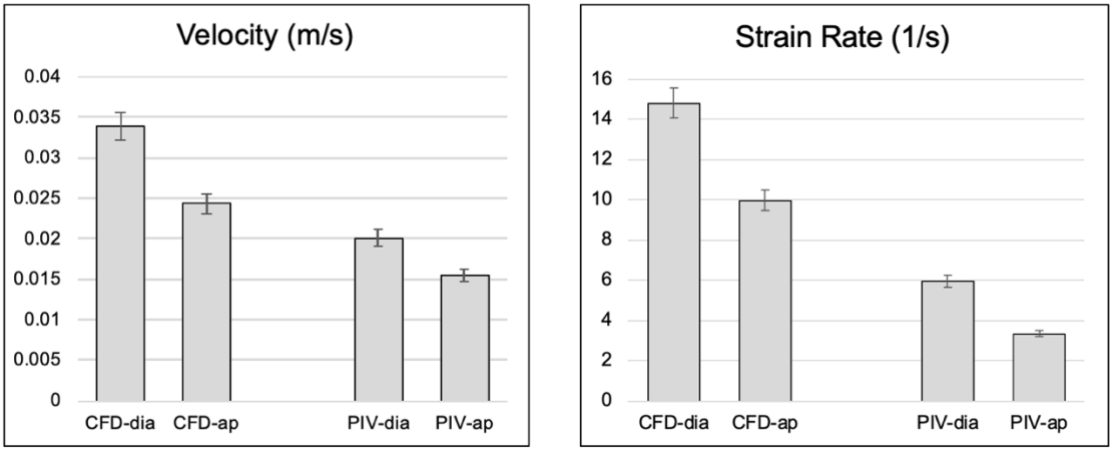

Figure 3-8: CFD vs. PIV Values – The apical configuration produced fluid with lower velocities and lower strain as evidenced by both CFD and PIV. PIV validated CFD trends; however, CFD values were consistently higher in magnitude regardless of configuration.

3.4. Discussion

Overall, PIV validated CFD trends but produced data that varied in value from CFD results. However, the data were not orders of magnitude in difference from each other, and instead only varied slightly. CFD consistently produced data with higher values in comparison with PIV suggesting the presence of systemic errors in either the CFD or PIV model. To improve results, the low-cost PIV system should be validated with a higher quality PIV machine such as a Dantec Dynamics or LAVision system [26]. This validation could lead to vital changes in the low-cost system that could reduce overall error. Regardless, PIV validated CFD results and was able to track flow within a deformable single ventricle using a low-cost patient-specific mock circulation loop.

3.5. References

[1] Morrison, T. M., Hariharan, P., Funkhouser, C. M., Afshari, P., Goodin, M., & Horner, M. (2019). Assessing Computational Model Credibility Using a Risk-Based Framework: Application to Hemolysis in Centrifugal Blood Pumps. In ASAIO Journal (Vol. 65, Issue 4, pp. 349–360). Ovid Technologies (Wolters Kluwer Health). https://doi.org/10.1097/mat.0000000000000996

[2] Malinauskas, R. A., Hariharan, P., Day, S. W., Herbertson, L. H., Buesen, M., Steinseifer, U., Aycock, K. I., Good, B. C., Deutsch, S., Manning, K. B., & Craven, B. A. (2017). FDA Benchmark Medical Device Flow Models for CFD Validation. In ASAIO Journal (Vol. 63, Issue 2, pp. 150–160). Ovid Technologies (Wolters Kluwer Health). https://doi.org/10.1097/mat.0000000000000499

[3] Cappon, F., Wu, T., Papaioannou, T., Du, X., Hsu, P.-L., & Khir, A. W. (2021). Mock circulatory loops used for testing cardiac assist devices: A review of computational and experimental models. In The International Journal of Artificial Organs (Vol. 44, Issue 11, pp. 793–806). SAGE Publications. https://doi.org/10.1177/03913988211045405

[4] Westerhof, N., Lankhaar, J.-W., & Westerhof, B. E. (2008). The arterial Windkessel. In Medical & Biological Engineering & Computing (Vol. 47, Issue 2, pp. 131–141). Springer Science and Business Media LLC. https://doi.org/10.1007/s11517-008-0359-2

[5] Pantalos, G. M., Koenig, S. C., Gillars, K. J., Giridharan, G. A., & Ewert, D. L. (2004). Characterization of an Adult Mock Circulation for Testing Cardiac Support Devices. In ASAIO Journal (Vol. 50, Issue 1, pp. 37–46). Ovid Technologies (Wolters Kluwer Health). https://doi.org/10.1097/01.mat.0000104818.70726.e6

[6] Giridharan, G. A., Ising, M., Sobieski, M. A., Koenig, S. C., Chen, J., Frankel, S., & Rodefeld, M. D. (2014). Cavopulmonary Assist for the Failing Fontan Circulation. In ASAIO Journal (Vol. 60, Issue 6, pp. 707–715). Ovid Technologies (Wolters Kluwer Health). https://doi.org/10.1097/mat.0000000000000135

[7] May-Newman, K., Marquez-Maya, N., Montes, R., & Salim, S. (2019). The Effect of Inflow Cannula Angle on the Intraventricular Flow Field of the Left Ventricular Assist Device–Assisted Heart: An In Vitro Flow Visualization Study. In ASAIO Journal (Vol. 65, Issue 2, pp. 139–147). Ovid Technologies (Wolters Kluwer Health). https://doi.org/10.1097/mat.0000000000000790

[8] May-Newman, K., Montes, R., Campos, J., Marquez-Maya, N., Vu, V., Zebrowski, E., Motomura, T., & Benkowski, R. (2019). Reducing regional flow stasis and improving

intraventricular hemodynamics with a tipless inflow cannula design: An in vitro flow visualization study using the EVAHEART LVAD. In Artificial Organs (Vol. 43, Issue 9, pp. 834–848). Wiley. https://doi.org/10.1111/aor.13477

[9] Viola, F., Jermyn, E., Warnock, J., Querzoli, G., & Verzicco, R. (2019). Left Ventricular Hemodynamics with an Implanted Assist Device: An In Vitro Fluid Dynamics Study. In Annals of Biomedical Engineering (Vol. 47, Issue 8, pp. 1799–1814). Springer Science and Business Media LLC. https://doi.org/10.1007/s10439-019-02273-6

[10] Khalafvand, S. S., Voorneveld, J. D., Muralidharan, A., Gijsen, F. J. H., Bosch, J. G., van Walsum, T., Haak, A., de Jong, N., & Kenjeres, S. (2018). Assessment of human left ventricle flow using statistical shape modelling and computational fluid dynamics. In Journal of Biomechanics (Vol. 74, pp. 116–125). Elsevier BV. https://doi.org/10.1016/j.jbiomech.2018.04.030

[11] Bazan, O., & Ortiz, J. P. (2016). Experimental validation of a cardiac simulator for in vitro evaluation of prosthetic heart valves. In Brazilian Journal of Cardiovascular Surgery. Sociedade Brasileira de Cirurgia Cardiovascular. https://doi.org/10.5935/1678-9741.20160041

[12] Sacco, F., Paun, B., Lehmkuhl, O., Iles, T. L., Iaizzo, P. A., Houzeaux, G., Vázquez, M., Butakoff, C., & Aguado-Sierra, J. (2018). Left Ventricular Trabeculations Decrease the Wall Shear Stress and Increase the Intra-Ventricular Pressure Drop in CFD Simulations. In Frontiers in Physiology (Vol. 9). Frontiers Media SA. https://doi.org/10.3389/fphys.2018.00458

[13] Doost, S. N., Ghista, D., Su, B., Zhong, L., & Morsi, Y. S. (2016). Heart blood flow simulation: a perspective review. In BioMedical Engineering OnLine (Vol. 15, Issue 1). Springer Science and Business Media LLC. https://doi.org/10.1186/s12938-016-0224-8

[14] Thielicke, W., & Stamhuis, E. J. (2014). PIVlab – Towards User-friendly, Affordable and Accurate Digital Particle Image Velocimetry in MATLAB. In Journal of Open Research Software (Vol. 2). Ubiquity Press, Ltd. https://doi.org/10.5334/jors.bl

[15] Ring, B. P., Atkinson, D. K., Henderson, A. W., & Lemley, E. C. (2013). Development of a Low Cost Particle Image Velocimetry System for Fluids Engineering Research and Education. In Volume 1A, Symposia: Advances in Fluids Engineering Education; Advances in Numerical Modeling for Turbomachinery Flow Optimization; Applications in CFD; Bio-Inspired Fluid Mechanics; CFD Verification and Validation; Development and Applications of Immersed Boundary Methods; DNS, LES, and Hybrid RANS/LES Methods. ASME 2013 Fluids Engineering Division Summer Meeting. American Society of Mechanical Engineers. https://doi.org/10.1115/fedsm2013-16239

[16] Ryerson, W. G., & Schwenk, K. (2011). A simple, inexpensive system for digital particle image velocimetry (DPIV) in biomechanics. In Journal of Experimental Zoology Part A: Ecological Genetics and Physiology (Vol. 317, Issue 2, pp. 127–140). Wiley. https://doi.org/10.1002/jez.725

[17] Fonseca, C. G., Backhaus, M., Bluemke, D. A., Britten, R. D., Chung, J. D., Cowan, B. R., Dinov, I. D., Finn, J. P., Hunter, P. J., Kadish, A. H., Lee, D. C., Lima, J. A. C., Medrano−Gracia, P., Shivkumar, K., Suinesiaputra, A., Tao, W., & Young, A. A. (2011). The Cardiac Atlas Project—an imaging database for computational modeling and

statistical atlases of the heart. In Bioinformatics (Vol. 27, Issue 16, pp. 2288–2295). Oxford University Press (OUP). https://doi.org/10.1093/bioinformatics/btr360

[18] Fedorov, A., Beichel, R., Kalpathy-Cramer, J., Finet, J., Fillion-Robin, J.-C., Pujol, S., Bauer, C., Jennings, D., Fennessy, F., Sonka, M., Buatti, J., Aylward, S., Miller, J. V., Pieper, S., & Kikinis, R. (2012). 3D Slicer as an image computing platform for the Quantitative Imaging Network. In Magnetic Resonance Imaging (Vol. 30, Issue 9, pp. 1323–1341). Elsevier BV. https://doi.org/10.1016/j.mri.2012.05.001

[19] Gregoric, I. D., Cohn, W. E., & Frazier, O. H. (2011). Diaphragmatic implantation of the HeartWare ventricular assist device. In The Journal of Heart and Lung Transplantation (Vol. 30, Issue 4, pp. 467–470). Elsevier BV. https://doi.org/10.1016/j.healun.2010.11.014

[20] Adamson, R. M., Mangi, A. A., Kormos, R. L., Farrar, D. J., & Dembitsky, W. P. (2014). Principles of HeartMate II Implantation to Avoid Pump Malposition and Migration. In Journal of Cardiac Surgery (Vol. 30, Issue 3, pp. 296–299). Wiley. https://doi.org/10.1111/jocs.12478

[21] Marechal, L., Balland, P., Lindenroth, L., Petrou, F., Kontovounisios, C., & Bello, F. (2021). Toward a Common Framework and Database of Materials for Soft Robotics. In Soft Robotics (Vol. 8, Issue 3, pp. 284–297). Mary Ann Liebert Inc. https://doi.org/10.1089/soro.2019.0115

[22] Westerhof, N., Lankhaar, J.-W., & Westerhof, B. E. (2008). The arterial Windkessel. In Medical & Biological Engineering & Computing (Vol. 47, Issue 2, pp. 131–141). Springer Science and Business Media LLC. https://doi.org/10.1007/s11517-008-0359-2

[23] Wong, K., Samaroo, G., Ling, I., Dembitsky, W., Adamson, R., del Álamo, J. C., & May-Newman, K. (2014). Intraventricular flow patterns and stasis in the LVAD-assisted heart. In Journal of Biomechanics (Vol. 47, Issue 6, pp. 1485–1494). Elsevier BV. https://doi.org/10.1016/j.jbiomech.2013.12.031

[24] Yazdi, S. G., Huetter, L., Docherty, P. D., Williamson, P. N., Clucas, D., Jermy, M., & Geoghegan, P. H. (2019). A Novel Fabrication Method for Compliant Silicone Phantoms of Arterial Geometry for Use in Particle Image Velocimetry of Haemodynamics. In Applied Sciences (Vol. 9, Issue 18, p. 3811). MDPI AG. https://doi.org/10.3390/app9183811

[25] Thielicke, W., & Sonntag, R. (2021). Particle Image Velocimetry for MATLAB: Accuracy and enhanced algorithms in PIVlab. In Journal of Open Research Software (Vol. 9). Ubiquity Press, Ltd. https://doi.org/10.5334/jors.334

[26] Adrian, R. J. (2005). Twenty years of particle image velocimetry. In Experiments in Fluids (Vol. 39, Issue 2, pp. 159–169). Springer Science and Business Media LLC. https://doi.org/10.1007/s00348-005-0991-7

4. PRACTICAL APPLICATION – AIM III

4.1. Introduction

Studies have shown that repetitive practice on realistic surgical models can improve surgeon technique [1-4]. This improvement has been observed in the congenital cardiac space, and is applicable to VAD implant training as VAD malpositioning remains a prevalent problem in medical device surgery [5-8]. Several notable innovations have occurred leading to an increase in congenital heart model realism. Mavroudis et al. achieved more realistic models by suturing formalin pig hearts into various configurations with congenital anomalies. Surgeons then practiced reconstructing the "congenital heart defect" cases [9]. Most notably, Yoo et al. 3D-printed their models with sophisticated techniques allowing high-detailed, immersive training [10]. Regardless of the technology used to create the synthetic hearts, physical surgical models have evolved to provide the tactile experience necessary for a realistic training experience.

Image guided surgery (IGS) has also been hypothesized to enhance surgeon technique [11]. IGS involves the use of tracked surgical instruments along with virtual images to guide surgical procedures [11]. Physical objects move in conjunction with paired virtual objects in real-time; the process works similarly to motion capture. Tracking markers can range from small simple spheres covered in reflective paint to electromagnetic markers [11]. Example applications of IGS include laparoscopic liver surgery and endoscopic sinus surgery [12,13]. It is important to note that IGS has minimally been used for thoracic procedures and has not yet been utilized for VAD surgery [14]. Furthermore, IGS is expensive (costing upwards of $300,000 for a single

system) and is difficult to use outside of the operating room [11,15]. Examples of current IGS systems used clinically include the Medtronic S7 StealthStation and the CAScination AG CAS-ONE Vario System [11]. Low-cost image-guided surgery systems do exist, but the platforms are experimental and require investigation [16-18].

Therefore, this work aims to create a novel IGS platform for VAD implant training. IGS is employed for both the apical and diaphragmatic implant techniques to emphasize the importance of an unobstructed inflow cannula when implanting a ventricular assist device.

4.2. Methods

A low-cost image guided surgery system was created using 3D Slicer IGT [16,17] and Plus Toolkit open source software [18]. Cardstock arUco tracking markers were used due to their affordability and widespread use [19,20]. Synthetic silicone hearts served as the physical heart models for implantation. Finally, a laptop with an external camera was used to capture the position of the tracking markers. Although the laptop internal camera can be used for acquisition, an external web camera allows the user more flexibility in positioning the camera while viewing the data on the computer screen. An overview of the proposed image guided surgery system is provided in Figure 4-1.

Two cases were investigated using image guided surgery. For the first case, a HLHS post-Fontan MRI was acquired from the Cardiac Atlas Project and the internal blood volume and myocardium were segmented using 3D Slicer [17]. The volume was then 3D-printed and used to cast synthetic heart models with Smooth-On Dragon Skin FX

Pro silicone [22,23] (Figure 4-2). Six hearts were casted in total. Three hearts were allocated for the control group and three hearts were reserved for the test group. Prior to physical implantation, a target cannula was virtually implanted in the diaphragmatic configuration of the virtual heart at Frazier's Point and served as the reference point for the physical implantations. For the control group, cannulas were implanted using traditional surgical methods. Reference images of the heart with Frazier's Point for diaphragmatic VAD placement were marked and a ruler was used to locate the point on the physical hearts. Silicone models were cored and inflow cannulas implanted. For the test group, cannulas were implanted using image guided surgery; a $20 GMESA external web camera was used for acquisition. Pivot calibration (0.2 mm RMSE) and model calibration (1.37 mm RMSE) were performed prior to implantation, and cannula-to-marker registration occurred manually. The virtual target cannula position was used to guide the physical implantation. The test cannulas were aligned with the target cannula using IGS, positions marked, the hearts cored, and cannulas implanted (Figure 4-3). For both the control and test groups, cannula positions were compared to the target cannula position using the Dice Similarity Coefficient for spatial overlap index (Equation 4-1) [25,26]. An overview of the difference between traditional and IGS methods is presented in Figure 4-4.

For the second case, two additional synthetic silicone hearts were casted. A cannula was implanted into the apex of the first heart using traditional surgical methods using a ruler and reference images as previously described. The second synthetic heart was used for image guided surgery; a $200 Intel RealSense D435 external web camera

was used for acquisition. Pivot calibration (0.31 mm RMSE) and model calibration (2.17 mm RMSE) were performed prior to implantation, and cannula-to-marker registration occurred manually. The virtual target cannula position was used to guide the physical implantation. The test cannulas were aligned with the target cannula using IGS, positions marked, the hearts cored, and cannulas implanted as previously described. For both the control and test groups, cannula positions were compared using computational fluid dynamics (CFD) with a specific focus on strain rate, velocity, and residence time [28,29,30].

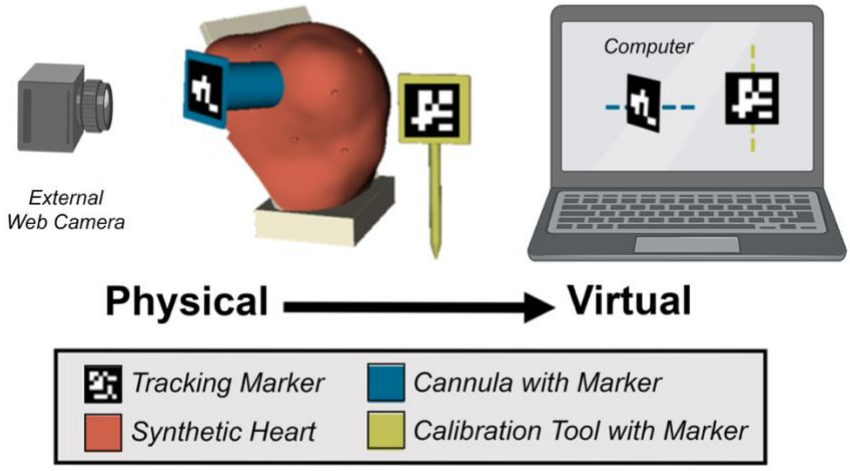

Figure 4-1: Image Guided Surgery Setup – The low-cost image guided surgery system was composed of a silicone heart model, laptop with external web camera, and arUco tracking markers.

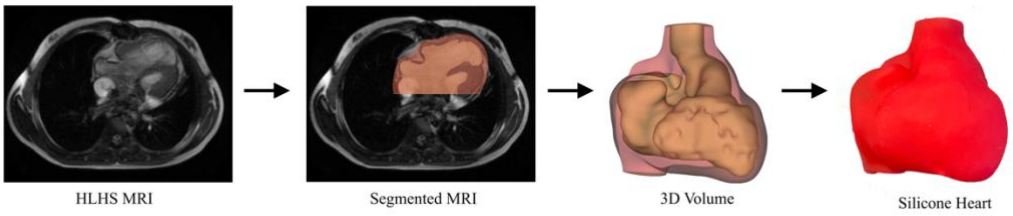

Figure 4-2: Silicone Heart Fabrication – A silicone synthetic heart was made from a HLHS MRI. The internal blood volume (orange) and myocardium (red) were segmented from the MRI, the 3D volumes were generated, and then molds were 3D-printed. Hearts were then casted with silicone for surgical training.

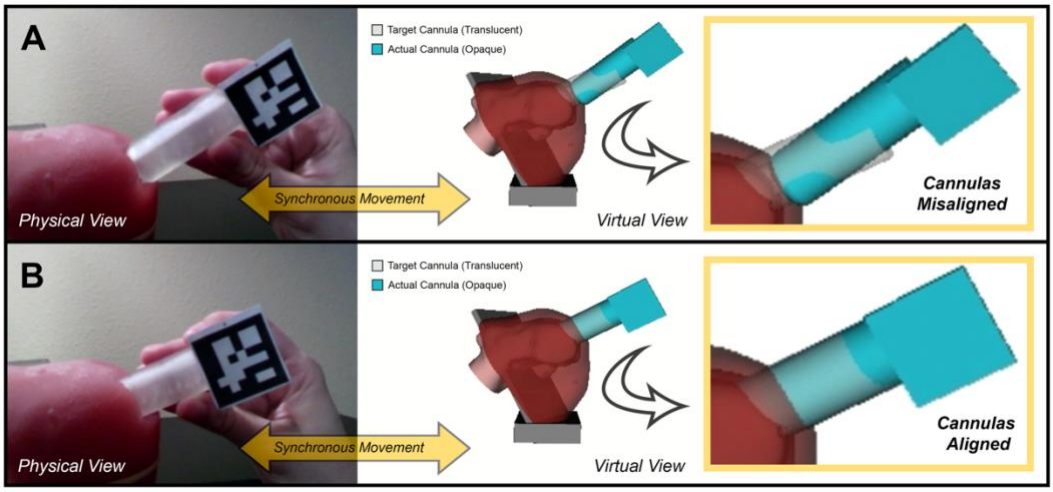

Figure 4-3: Image Guided Surgery Implant Process – Image guided surgery pairs the physical domain with the virtual domain using tracking markers. As the physical cannula is moved, the virtual cannula (opaque blue) moves in real-time. The test cannula (opaque blue) is misaligned with the target cannula (translucent gray) (A). After readjustment, the test cannula (opaque blue) is aligned with the target cannula (translucent gray) (B), and implantation can occur.

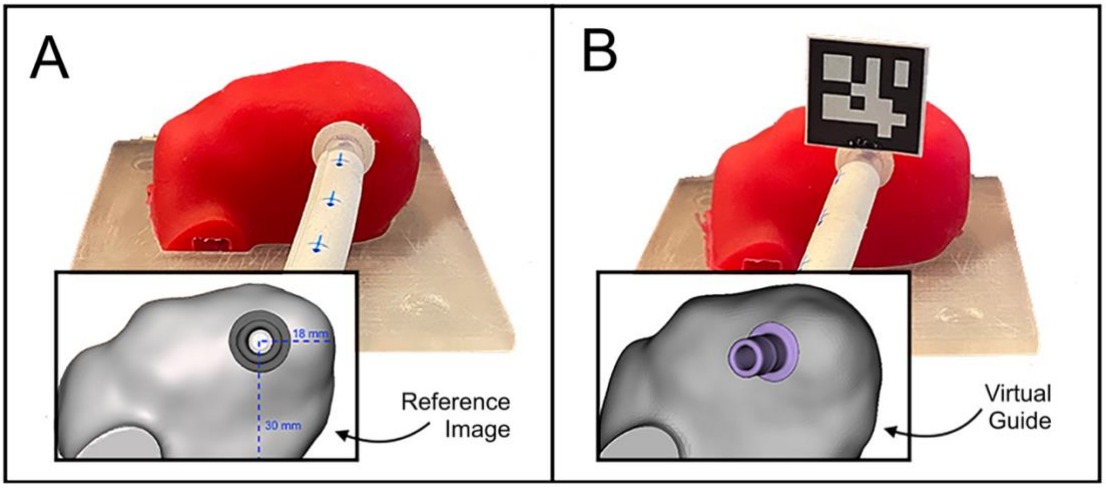

Figure 4-4: Traditional vs. Proposed Implant Technique – The traditional method of VAD implantation involves using a reference image to make measurements for inflow cannula placement (A). The proposed method is image guided surgery that uses tracking markers and a target cannula (purple) to guide the implant procedure (B).

Equation 4-1: Dice Similarity Coefficient (DSC) = $\frac{\mathbf{2}|\boldsymbol{X}\cap\boldsymbol{Y}|}{|\boldsymbol{X}|+|\boldsymbol{Y}|}$,
where X is the observed cannula position and Y is the target cannula position.

4.3. Results

For the first case of diaphragmatic implants, the cannulas from the control group had poor spatial overlap with the target cannula (Figure 4-5A). The average dice similarity coefficient (DSC) between the control group cannulas and target cannula was 14.8 +/- 4.5%. The cannulas from the test group implanted using image guided surgery exhibited greater spatial overlap with the target cannula (Figure 4-5B). The average DSC between the test group cannulas and target cannula was 58.6 +/- 8.0%. Upon visual inspection, it is clear that cannulas implanted with IGS were positioned closer to the target cannula in comparison to the cannulas implanted by traditional means (Figure 4-5). Of note, inflow cannula obstruction was commonly observed for the control group (Figure 4-6).

Similar results were observed for the second case with the apical implants. The control cannula was malpositioned while the test cannula was placed centrally within the ventricle, free from obstruction (Figure 4-7). CFD revealed a focal region of low-velocity (<0.09 m/s), high strain rate (~700/s) fluid within the wedge region of the ventricle near the device-tissue interface for the control case. The fluid in this area also exhibited residence times of approximately 3.8 seconds. The hemodynamic conditions for the IGS case were less prone to thrombosis. Fluid near the implant site featured higher velocity (~0.18 m/s), improved strain rate (>250/s, <400/s) flow with shorter residence times (~1.8 s). Figure 4-8 compares CFD results for the control and test cases.

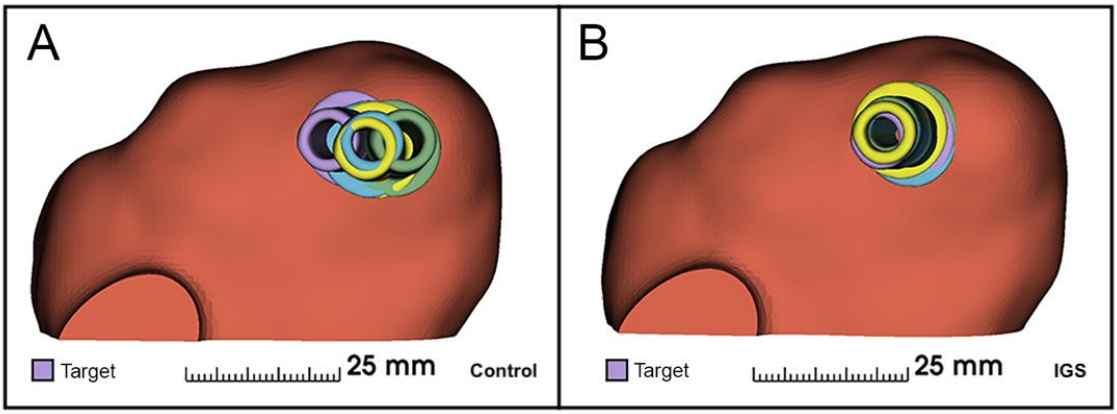

Figure 4-5: Traditional vs. IGS Implantation Results – The control cannulas (blue, yellow, green) were implanted far from the target cannula (purple) (A). The test cannulas (blue, yellow, green) implanted using IGS were positioned closer to the target cannula (purple) (B).

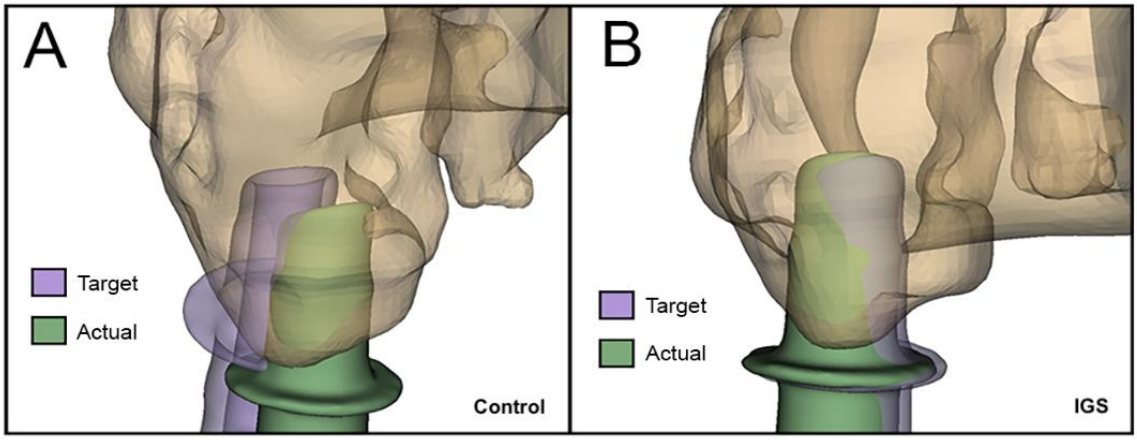

Figure 4-6: Inflow Cannula Obstruction – Control cannulas (green) were not implanted near the target cannula (purple) and resulted in inflow cannula obstruction (A). Test cannulas (green) were implanted closer to the target cannula (purple) and did not result in inflow cannula obstruction (B).

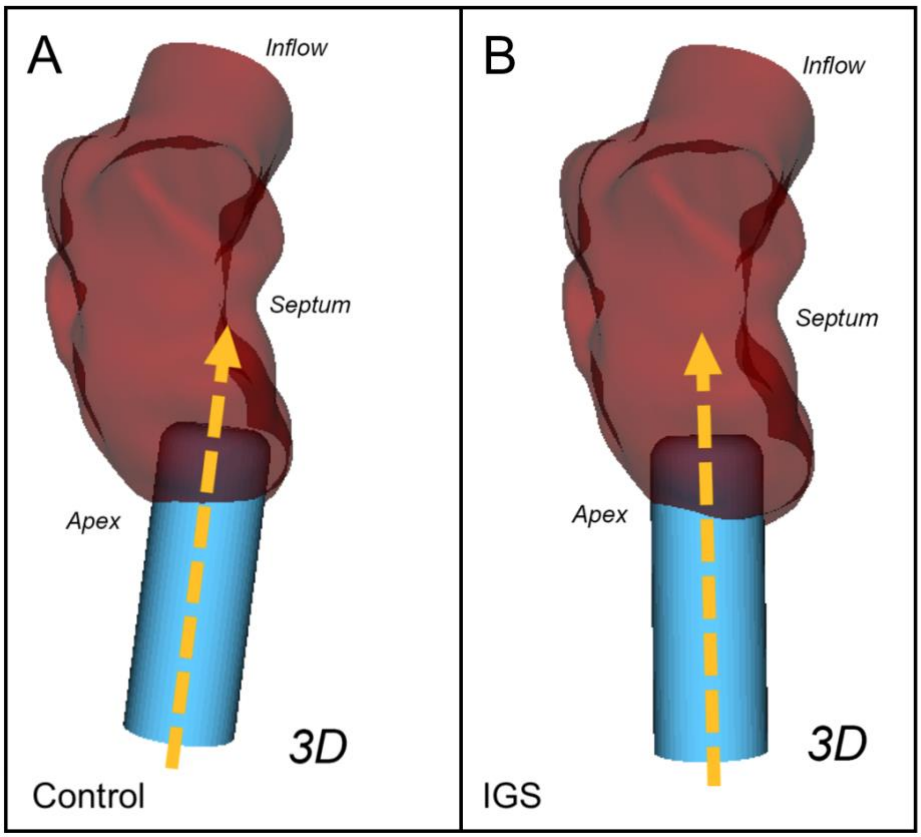

Figure 4-7: Inflow Cannula Malangulation – Cannulas implanted with the control technique resulted in an obstructed inflow (A). Cannulas implanted with IGS exhibited a more central implant location free from inflow obstruction (B).

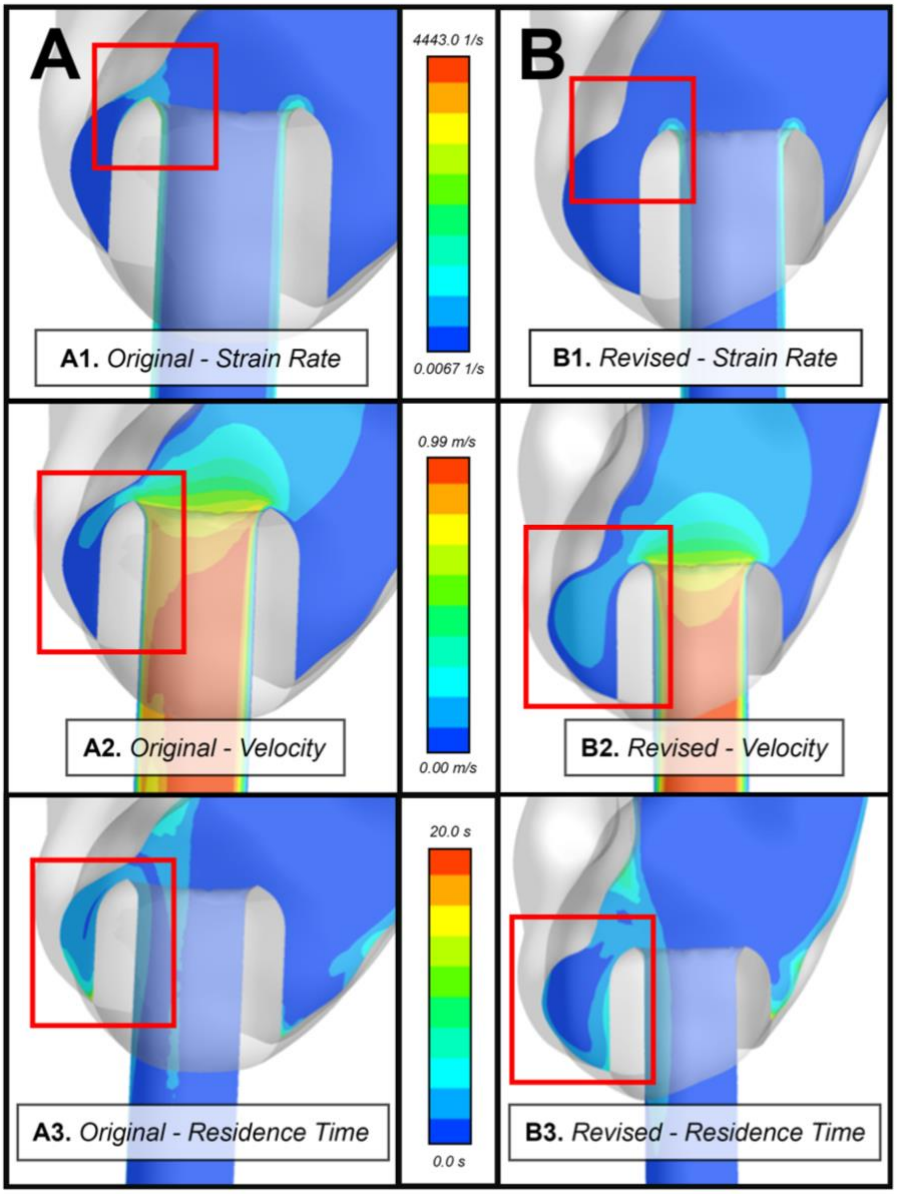

Figure 4-8: CFD Results for Traditional vs. IGS Implant Technique – CFD revealed a focal region of high strain rate, low velocity fluid with long residence time for the control implant (A). The IGS implant exhibited improved hemodynamics with less thrombogenic potential (B). Fluid in this region featured normal strain rates, higher velocities, and shorter residence times.

4.4. Discussion

For both the diaphragmatic and apical cases, image guided surgery produced cannula positions closer to the target cannula. The target cannula was optimally placed prior to implantation using virtual surgery; therefore, it served as an excellent guide to avoid the dense trabeculations within the patient ventricle upon implantation. Cannulas implanted with the traditional method without the target cannula as a guide were therefore prone to inflow cannula obstruction. Consequently, the use of IGS has the potential to improve VAD cannula implant positioning and even minimize thrombogenic potential as suggested by the CFD results. Optimal placement of VAD inflow cannulas could also lead to reduced suction events, and the technique itself could lead to reduced operating time and need for surgical revision (i.e., pump exchange due to thrombotic events).

This work could be improved by validating the low-cost image guided surgery platform. Although a series of calibrations were performed, the system itself could be validated by more advanced technology such as Medtronic's S7 StealthStation or the more economical OptiTrack Duo [31]. An additional external web camera could also be added to provide another point of reference for marker tracking. Additionally, more cases should be performed to explore the limits of IGS for VAD implantation. The CFD model to analyze implant results could also be improved. Currently, it takes weeks to months to generate a solution. However, real-time CFD could provide more meaningful results, especially in a clinical setting. Although real-time CFD has not yet been developed for blood flow, ANSYS has created Discovery Live to accommodate real-time results for basic air and water fluid flow problems [32-35]. This technology is promising, and if

translatable to blood flow, could serve as a useful tool for analyzing inflow cannula placement after image guided surgery.

4.5. References

[1] Trehan, K., Kemp, C. D., & Yang, S. C. (2014). Simulation in cardiothoracic surgical training: Where do we stand? In The Journal of Thoracic and Cardiovascular Surgery (Vol. 147, Issue 1, pp. 18-24.e2). Elsevier BV. https://doi.org/10.1016/j.jtcvs.2013.09.007

[2] Yanagawa, B., Ribeiro, R., Naqib, F., Fann, J., Verma, S., & Puskas, J. D. (2019). See one, simulate many, do one, teach one. In Current Opinion in Cardiology (Vol. 34, Issue 5, pp. 571–577). Ovid Technologies (Wolters Kluwer Health). https://doi.org/10.1097/hco.0000000000000659

[3] Feins, R. H., Burkhart, H. M., Conte, J. V., Coore, D. N., Fann, J. I., Hicks, G. L., Jr., Nesbitt, J. C., Ramphal, P. S., Schiro, S. E., Shen, K. R., Sridhar, A., Stewart, P. W., Walker, J. D., & Mokadam, N. A. (2017). Simulation-Based Training in Cardiac Surgery. In The Annals of Thoracic Surgery (Vol. 103, Issue 1, pp. 312–321). Elsevier BV. https://doi.org/10.1016/j.athoracsur.2016.06.062

[4] Burkhart, H. M., Riley, J. B., Hendrickson, S. E., Glenn, G. F., Lynch, J. J., Arnold, J. J., Dearani, J. A., Schaff, H. V., & Sundt, T. M., III. (2010). The successful application of simulation-based training in thoracic surgery residency. In The Journal of Thoracic and Cardiovascular Surgery (Vol. 139, Issue 3, pp. 707–712). Elsevier BV. https://doi.org/10.1016/j.jtcvs.2009.10.029

[5] Burkhart, H. M. (2017). Simulation in congenital cardiac surgical education: We have arrived. In The Journal of Thoracic and Cardiovascular Surgery (Vol. 153, Issue 6, pp. 1528–1529). Elsevier BV. https://doi.org/10.1016/j.jtcvs.2017.03.012

[6] Sorensen, E. N., Hiivala, N. J., Jeudy, J., Rajagopal, K., & Griffith, B. P. (2013). Computed tomography correlates of inflow cannula malposition in a continuous-flow ventricular-assist device. In The Journal of Heart and Lung Transplantation (Vol. 32, Issue 6, pp. 654–657). Elsevier BV. https://doi.org/10.1016/j.healun.2013.03.010.

[7] Kneebone, R. L., Nestel, D., Vincent, C., & Darzi, A. (2007). Complexity, risk and simulation in learning procedural skills. In Medical Education (Vol. 41, Issue 8, pp. 808–814). Wiley. https://doi.org/10.1111/j.1365-2923.2007.02799.x.

[8] Han, J. J., & Patrick, W. L. (2019). See one—practice—do one—practice—teach one—practice: The importance of practicing outside of the operating room in surgical training. In The Journal of Thoracic and Cardiovascular Surgery (Vol. 157, Issue 2, pp. 671–677). Elsevier BV. https://doi.org/10.1016/j.jtcvs.2018.07.108.

[9] Mavroudis, C. D., Mavroudis, C., Jacobs, J. P., DeCampli, W. M., & Tweddell, J. S. (2018). Simulation and Deliberate Practice in a Porcine Model for Congenital Heart Surgery Training. In The Annals of Thoracic Surgery (Vol. 105, Issue 2, pp. 637–643). Elsevier BV. https://doi.org/10.1016/j.athoracsur.2017.10.011.

[10] Yoo, S.-J., Spray, T., Austin, E. H., III, Yun, T.-J., & van Arsdell, G. S. (2017). Hands-on surgical training of congenital heart surgery using 3-dimensional print models. In The Journal of Thoracic and Cardiovascular Surgery (Vol. 153, Issue 6, pp. 1530–1540). Elsevier BV. https://doi.org/10.1016/j.jtcvs.2016.12.054.

[11] Azagury, D. E., Dua, M. M., Barrese, J. C., Henderson, J. M., Buchs, N. C., Ris, F., Cloyd, J. M., Martinie, J. B., Razzaque, S., Nicolau, S., Soler, L., Marescaux, J., & Visser, B. C. (2015). Image-guided surgery. In Current Problems in Surgery (Vol. 52, Issue 12, pp. 476–520). Elsevier BV. https://doi.org/10.1067/j.cpsurg.2015.10.001

[12] Prevost, G. A., Eigl, B., Paolucci, I., Rudolph, T., Peterhans, M., Weber, S., Beldi, G., Candinas, D., & Lachenmayer, A. (2019). Efficiency, Accuracy and Clinical Applicability of a New Image-Guided Surgery System in 3D Laparoscopic Liver Surgery. In Journal of Gastrointestinal Surgery (Vol. 24, Issue 10, pp. 2251–2258). Springer Science and Business Media LLC. https://doi.org/10.1007/s11605-019-04395-7

[13] Ramakrishnan, V. R., Orlandi, R. R., Citardi, M. J., Smith, T. L., Fried, M. P., & Kingdom, T. T. (2012). The use of image-guided surgery in endoscopic sinus surgery: an evidence-based review with recommendations. In International Forum of Allergy & Rhinology (Vol. 3, Issue 3, pp. 236–241). Wiley. https://doi.org/10.1002/alr.21094

[14] Dilley, J., Camara, M., Omar, I., Carter, A., Pratt, P., Vale, J., Darzi, A., & Mayer, E. K. (2019). Evaluating the impact of image guidance in the surgical setting: a systematic review. In Surgical Endoscopy (Vol. 33, Issue 9, pp. 2785–2793). Springer Science and Business Media LLC. https://doi.org/10.1007/s00464-019-06876-x

[15] Wang, J. C., Nagy, L., & Demke, J. C. (2015). Image-guided surgery and craniofacial applications: mastering the unseen. In Maxillofacial Plastic and Reconstructive Surgery (Vol. 37, Issue 1). Springer Science and Business Media LLC. https://doi.org/10.1186/s40902-015-0037-x

[16] Ungi, T., Sargent, D., Moult, E., Lasso, A., Pinter, C., McGraw, R. C., & Fichtinger, G. (2012). Perk Tutor: An Open-Source Training Platform for Ultrasound-Guided Needle Insertions. In IEEE Transactions on Biomedical Engineering (Vol. 59, Issue 12, pp. 3475–3481). Institute of Electrical and Electronics Engineers (IEEE). https://doi.org/10.1109/tbme.2012.2219307

[17] Fedorov, A., Beichel, R., Kalpathy-Cramer, J., Finet, J., Fillion-Robin, J.-C., Pujol, S., Bauer, C., Jennings, D., Fennessy, F., Sonka, M., Buatti, J., Aylward, S., Miller, J. V., Pieper, S., & Kikinis, R. (2012). 3D Slicer as an image computing platform for the Quantitative Imaging Network. In Magnetic Resonance Imaging (Vol. 30, Issue 9, pp. 1323–1341). Elsevier BV. https://doi.org/10.1016/j.mri.2012.05.001

[18] Lasso, A., Heffter, T., Rankin, A., Pinter, C., Ungi, T., & Fichtinger, G. (2014). PLUS: Open-Source Toolkit for Ultrasound-Guided Intervention Systems. In IEEE Transactions on Biomedical Engineering (Vol. 61, Issue 10, pp. 2527–2537). Institute of Electrical and Electronics Engineers (IEEE). https://doi.org/10.1109/tbme.2014.2322864

[19] Romero-Ramirez, F. J., Muñoz-Salinas, R., & Medina-Carnicer, R. (2018). Speeded up detection of squared fiducial markers. In Image and Vision Computing (Vol. 76, pp. 38–47). Elsevier BV. https://doi.org/10.1016/j.imavis.2018.05.004

[20] Garrido-Jurado, S., Muñoz-Salinas, R., Madrid-Cuevas, F. J., & Medina-Carnicer, R. (2016). Generation of fiducial marker dictionaries using Mixed Integer Linear Programming. In Pattern Recognition (Vol. 51, pp. 481–491). Elsevier BV. https://doi.org/10.1016/j.patcog.2015.09.023

[21] Fonseca, C. G., Backhaus, M., Bluemke, D. A., Britten, R. D., Chung, J. D., Cowan, B. R., Dinov, I. D., Finn, J. P., Hunter, P. J., Kadish, A. H., Lee, D. C., Lima, J. A. C., Medrano−Gracia, P., Shivkumar, K., Suinesiaputra, A., Tao, W., & Young, A. A. (2011). The Cardiac Atlas Project—an imaging database for computational modeling and statistical atlases of the heart. In Bioinformatics (Vol. 27, Issue 16, pp. 2288–2295). Oxford University Press (OUP). https://doi.org/10.1093/bioinformatics/btr360

[22] Yan, D., & McQueen, A. (2020). No oranges, bananas or chicken: a simulated suturing model. In BMJ Simulation and Technology Enhanced Learning (Vol. 6, Issue 5, pp. 316–316). BMJ. https://doi.org/10.1136/bmjstel-2019-000477

[23] Marechal, L., Balland, P., Lindenroth, L., Petrou, F., Kontovounisios, C., & Bello, F. (2021). Toward a Common Framework and Database of Materials for Soft Robotics. In Soft Robotics (Vol. 8, Issue 3, pp. 284–297). Mary Ann Liebert Inc. https://doi.org/10.1089/soro.2019.0115

[24] Gregoric, I. D., Cohn, W. E., & Frazier, O. H. (2011). Diaphragmatic implantation of the HeartWare ventricular assist device. In The Journal of Heart and Lung Transplantation (Vol. 30, Issue 4, pp. 467–470). Elsevier BV. https://doi.org/10.1016/j.healun.2010.11.014

[25] Thada, Vikas & Jaglan, Vivek. (2013). Comparison of Jaccard, Dice, Cosine Similarity Coefficient To Find Best Fitness Value for Web Retrieved Documents Using Genetic Algorithm. International Journal of Innovations in Engineering and Technology. 2. 202-205.

[26] Zou, K. H., Warfield, S. K., Bharatha, A., Tempany, C. M. C., Kaus, M. R., Haker, S. J., Wells, W. M., III, Jolesz, F. A., & Kikinis, R. (2004). Statistical validation of image segmentation quality based on a spatial overlap index1. In Academic Radiology (Vol. 11, Issue 2, pp. 178–189). Elsevier BV. https://doi.org/10.1016/s1076-6332(03)00671-8

[27] Adamson, R. M., Mangi, A. A., Kormos, R. L., Farrar, D. J., & Dembitsky, W. P. (2014). Principles of HeartMate II Implantation to Avoid Pump Malposition and Migration. In Journal of Cardiac Surgery (Vol. 30, Issue 3, pp. 296–299). Wiley. https://doi.org/10.1111/jocs.12478

[28] Fraser, K. H., Zhang, T., Taskin, M. E., Griffith, B. P., & Wu, Z. J. (2010). Computational Fluid Dynamics Analysis of Thrombosis Potential in Left Ventricular Assist Device Drainage Cannulae. In ASAIO Journal (Vol. 56, Issue 3, pp. 157–163). Ovid Technologies (Wolters Kluwer Health). https://doi.org/10.1097/mat.0b013e3181d861f1

[29] Liao, S., Neidlin, M., Li, Z., Simpson, B., & Gregory, S. D. (2018). Ventricular flow dynamics with varying LVAD inflow cannula lengths: In-silico evaluation in a multiscale model. In Journal of Biomechanics (Vol. 72, pp. 106–115). Elsevier BV. https://doi.org/10.1016/j.jbiomech.2018.02.038

[30] Liao, S., Simpson, B., Neidlin, M., Kaufmann, T. A. S., Li, Z., Woodruff, M. A., & Gregory, S. D. (2016). Numerical prediction of thrombus risk in an anatomically dilated left ventricle: the effect of inflow cannula designs. In BioMedical Engineering OnLine (Vol. 15, Issue S2). Springer Science and Business Media LLC. https://doi.org/10.1186/s12938-016-0262-2

[31] Pérez-Castilla, A., Piepoli, A., Delgado-García, G., Garrido-Blanca, G., & García-Ramos, A. (2019). Reliability and Concurrent Validity of Seven Commercially Available Devices for the Assessment of Movement Velocity at Different Intensities During the Bench Press. In Journal of Strength and Conditioning Research (Vol. 33, Issue 5, pp. 1258–1265). Ovid Technologies (Wolters Kluwer Health). https://doi.org/10.1519/jsc.0000000000003118

[32] Fleischmann, C., Leher, I., Hartwich, R., Hainke, M., & Sesselmann, S. (2019). A new approach to quickly edit geometries and estimate stresses and displacements of implants in real-time. In Current Directions in Biomedical Engineering (Vol. 5, Issue 1, pp. 553–556). Walter de Gruyter GmbH. https://doi.org/10.1515/cdbme-2019-0139

[33] Huang, H., Yin, H., Wang, Y., Chen, N., Huang, D., Luo, X., Yin, X., Zheng, Q., Shi, B., & Li, J. (2019). Computational Fluid Dynamic Analysis of Different Velopharyngeal Closure Patterns. In Annals of Otology, Rhinology & Laryngology (Vol. 129, Issue 2, pp. 157–163). SAGE Publications. https://doi.org/10.1177/0003489419879176

[34] He, X., & Luo, L.-S. (1997). Lattice Boltzmann Model for the Incompressible Navier–Stokes Equation. In Journal of Statistical Physics (Vol. 88, Issue 3/4, pp. 927–944). Springer Science and Business Media LLC. https://doi.org/10.1023/b:joss.0000015179.12689.e4

[35] Chen, S., & Doolen, G. D. (1998). LATTICE BOLTZMANN METHOD FOR FLUID FLOWS. In Annual Review of Fluid Mechanics (Vol. 30, Issue 1, pp. 329–364). Annual Reviews. https://doi.org/10.1146/annurev.fluid.30.1.329

5. CONCLUSIONS

Overall, this work aims to investigate the relationship between ventricular assist device inflow cannula configuration and thrombus formation within single ventricle hearts. A novel dynamic computational model was used to identify regions of potential thrombosis risk and was validated by particle image velocimetry using a patient-specific mock circulation loop. Finally, inflow cannula position was optimized through a new surgical technique involving a low-cost image guided surgery system.

More specifically, the concept of computational fluid dynamics (CFD) was introduced and a novel computational model with a patient-specific moving mesh was presented. It was hypothesized that implant configuration affects thrombus formation. CFD results showed that VAD implant position influenced thrombogenic potential within single ventricle hearts. In fact, the apical implant configuration produced a greater volume of regions with thrombosis risk in comparison to the diaphragmatic implant configuration.

CFD results were then validated using a novel mock circulation loop and low-cost particle image velocimetry (PIV) system. The mock circulation loop consisted of an optically clear deformable patient-specific ventricular sac within a pressure tank, reservoir, compliance chamber, and resistance element. Pre-VAD support and VAD support conditions were successfully modeled and PIV confirmed trends found in the computational studies. However, PIV results were consistently lower in value compared to CFD results, suggesting the need to refine both models.

Finally, a practical application was introduced involving low-cost image guided surgery. It was hypothesized that image guided surgery (IGS) improves VAD implant

positioning. The difference in implant position using traditional surgical methods vs. IGS was compared. IGS resulted in inflow cannula placements closer to the target cannula. Furthermore, cannulas implanted with this technique demonstrated reduced thrombosis risk and unobstructed inflows.

Ultimately, this work presents several novel concepts in terms of computational, experimental, and applicable research ideas, and aims to solve real-world surgical issues relevant to the field of ventricular assist device medical implants. Future work should focus on refining both the computational and experimental benchtop models, and validating the low-cost image guided and particle velocimetry systems. Additionally, more cases should be studied beyond HLHS as this work can be translated to other populations of patients in need of VAD support.